

# The Earthquake Cycle in the San Francisco Bay Region: A.D. 1600–2012

by David P. Schwartz, James J. Lienkaemper, Suzanne Hecker, Keith I. Kelson, Thomas E. Fumal,\* John N. Baldwin, Gordon G. Seitz, and Tina M. Niemi

**Abstract** Stress changes produced by the 1906 San Francisco earthquake had a profound effect on the seismicity of the San Francisco Bay region (SFBR), dramatically reducing it in the twentieth century. Whether the SFBR is still within or has emerged from this seismic quiescence is an issue of debate with implications for earthquake mechanics and seismic hazards. Historically, the SFBR has not experienced one complete earthquake cycle (i.e., the accumulation of stress, its release primarily as coseismic slip during surface-faulting earthquakes, its re-accumulation in the interval following, and its subsequent rerelease). The historical record of earthquake occurrence in the SFBR appears to be complete at about  $M$  5.5 back to 1850 (Bakun, 1999). For large events, the record may be complete back to 1776, which represents about half a cycle. Paleoseismic data provide a more complete view of the most recent pre-1906 SFBR earthquake cycle, extending it back to about 1600. Using these, we have developed estimates of magnitude and seismic moment for alternative sequences of surface-faulting paleoearthquakes occurring between 1600 and 1776 on the region's major faults. From these we calculate seismic moment and moment release rates for different time intervals between 1600 and 2012. These show the variability in moment release and suggest that, in the SFBR regional plate boundary, stress can be released on a single fault in great earthquakes such as that in 1906 and in multiple ruptures distributed on the regional plate boundary fault system on a decadal time scale.

## Introduction

The earthquake cycle paradigm (the accumulation of stress, its release as slip on a fault or a set of faults, and its re-accumulation) has long been of interest to earthquake scientists. It provides a broad framework for developing an understanding of repeated behavior of faults and fault systems and has implications for evaluating likely future rupture occurrence. Its roots lie in observations such as those of Gilbert (1884) for fault scarps in the Basin and Range and of the 1872 earthquake and surface rupture. In his explanation of mountain building, he states “Suddenly, and almost instantaneously, there is an amount of motion sufficient to relieve the strain, and this is followed by a long period of quiet, during which the strain is gradually reimposed.” This prescient interpretation of Earth behavior reached early maturation with the Reid (1910) formalization of elastic rebound following geologic and geodetic observations made of the 1906  $M$  7.9 San Francisco, California, earthquake. The concept of the earthquake cycle has been applied to earthquake recurrence on individual faults, as well as to an assemblage of faults in a region. Interpretations of regional cycles are primarily based on historical seismicity catalogs, from which it has been suggested that an earthquake sequence,

which is initiated by the occurrence of a great earthquake, is followed first by a reduction in the rate of regional seismicity and then by the acceleration of regional moment release preceding the next large or great event (Ellsworth *et al.*, 1981; Sykes and Jaume, 1990; Bakun, 1999; Bowman and King, 2001; Bebbington *et al.*, 2010). This perspective on the earthquake cycle is extremely important but has temporal limitations in that full cycles, at least in regions of shallow continental crust, have rarely, if ever, been documented. In most seismically active areas, many of the principal faults have not failed historically, let alone repeatedly. In this paper, we present a longer-term view of the earthquake cycle for the San Francisco Bay region (SFBR) by expanding the earthquake timeline back to approximately A.D. 1600 (hereafter all dates are A.D.) through the dating of paleoearthquakes on the region's major faults.

The SFBR is defined as the area within the rectangle in Figure 1 following the regional seismicity analysis of Bakun (1999) and usage adopted by the Working Group on California Earthquake Probabilities (WGCEP, 1999, 2003, 2008). The SFBR is within the boundary between the Pacific and North American plates. Plate boundary slip is accommodated by the coseismic offset, and to a lesser extent by creep, along the region's principal faults: the San Andreas,

\*Deceased (2010).

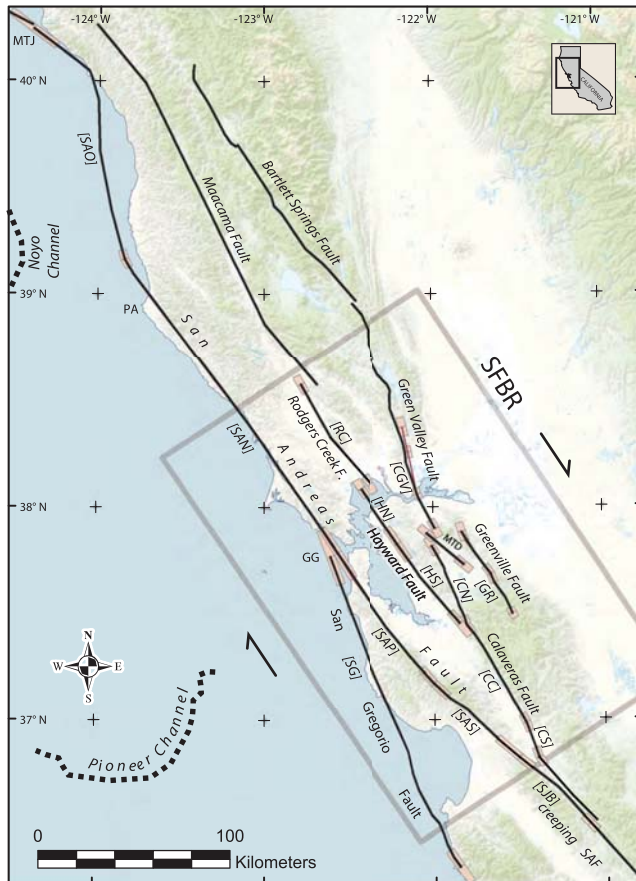


**Figure 1.** Map of principal plate boundary faults in the San Francisco Bay region (SFBR) and northern California. The rectangle encloses the area defined as the SFBR, which was developed by Bakun (1999) for his analysis of historical seismicity and used by the WGCEP (1999, 2003, 2008) to evaluate SFBR earthquake probabilities. Arrows indicate relative direction of plate movement. Fault segmentation is from WGCEP (2003), with addition of the San Juan Bautista (SJB) segment in the present analysis. Segment acronyms and associated segment names are listed in Table 1. MTJ, Mendocino triple junction; PA, Point Arena; and GG, Golden Gate.

San Gregorio, Calaveras, Hayward–Rodgers Creek, Greenville, and Concord–Green Valley faults (Fig. 1, Table 1). The SFBR is a natural laboratory to assess earthquake cycles on a regional scale because (a) the distribution of the plate boundary strike-slip faults that release essentially all of the accumulated seismic moment from plate motions is well known; (b) short- and long-term plate rates have been geologically and geodetically measured; (c) there is information on the historical seismic record back to the early–mid 1800s; and (d) a paleoearthquake chronology is emerging that permits extension of the timeline of large earthquakes to precede the historical record.

The tectonic loading or slip rate across the SFBR from plate motions appears generally constant, within uncertainties, over widely varying intervals of time. The budget between what goes into the system as stress and what comes out as earthquakes is an important element of the earthquake cycle. On a long-term basis, slip from the Nuvel 1A plate

**Table 1**

List of San Francisco Bay Region (SFBR) Faults and Fault Segments

Fault/Segment	Acronyms*
San Andreas Offshore	SAO
San Andreas North Coast	SAN
San Andreas Peninsula	SAP
San Andreas Santa Cruz Mountains	SAS
San Andreas San Juan Bautista	SJB
San Gregorio	SG
Rodgers Creek	RC
Hayward North	HN
Hayward South	HS
Calaveras North	CN
Calaveras Central	CC
Calaveras South	CS
Concord–Green Valley	CGV
Mount Diablo	MTD
Greenville	GR

\*Fault and fault segment acronyms are used in figures and in tables. Segments are shown in Figure 1.

model averages  $41 \pm 4$  mm/yr for the past four million years (DeMets *et al.*, 1994). Geologic slip rates for the past several hundred to several thousand years obtained from SFBR faults give a rate of 36–43 mm/yr when summed across the region (WGCEP, 2003). The short-term geodetic rate derived from measurements made from 1993 to 2003 is  $37 \pm 0.6$  mm/yr (d'Alessio *et al.*, 2005). Although the similarity in rates over these three very different timescales could be fortuitous, it is likely that given the overall size of the fault system that passes through the region, the tectonic stressing rate has been essentially constant for the time interval of interest in our analysis.

Historically, the SFBR has not experienced a complete earthquake cycle, which classically has been considered as the interval between repeats of the great 1906 rupture of the San Andreas fault (Ellsworth *et al.*, 1981). The record of earthquakes of  $M \geq 5.5$  appears to be complete back to 1850 (Bakun, 1999), which is only part of a cycle. Topozada and Borchardt (1998) suggest that for large events ( $M \sim 7$ ), the record is complete to 1776, which is the beginning of construction of Spanish Missions in the SFBR. From 1776 through the present, surface rupture may have occurred along a section of the San Andreas fault in 1838 (Appendix A); however, only the southern Hayward (HS) fault in 1868 and the full northern San Andreas fault in 1906 can be definitively identified as having produced large surface ruptures.

Paleoseismic observations provide information on the timing of surface-faulting earthquakes prior to, and in some cases during the early part of, the historical record. These form the core of our analysis. Because of uncertainties inherent in dating paleoearthquakes, alternative surface-rupture sequences are developed for the major faults for the 1600–1776 interval and for the shorter 1690–1776 interval. For each paleoearthquake in these models, we estimate the magnitude and seismic moment of the associated paleoearthquake based on (with minor modifications) the seismic source

characterization developed by the WGCEP (2003). The resulting paleoseismic record and the historical seismic record are used to develop two models of the earthquake cycle in terms of seismic moment release during different intervals of time in the 412-year period from 1600 to 2012. One model is based solely on the occurrence of paleoseismic and historical surface ruptures. The other combines these with the occurrence of historical  $M \leq 5 + M \geq 5.5$  earthquakes (Bakun, 1999). Seismic moment release in the SFBR is then discussed in the context of the earthquake cycle, showing that it occurs in multiple modes. Finally, the implications of our interpretations for seismic hazard in the SFBR are presented.

## Expanding the SFBR Earthquake Catalog

### Key Timelines

There are three key timelines that provide information on the occurrence of SFBR earthquakes. These are (1) the historical record of moderate magnitude events, (2) the historical record of large magnitude earthquakes, and (3) the paleoseismic record of surface-faulting earthquakes.

Bakun (1999) is the primary source of information on historical Bay Area seismicity, including estimates of seismic moment release prior to and following the 1906 earthquake. In analyzing available information on shaking intensity, he developed a catalog of SFBR earthquakes that extends back to 1836. It includes preinstrumental magnitude estimates using modified Mercalli intensity values to produce an intensity magnitude ( $M_I$ ) that is calibrated to moment magnitude (Bakun and Wentworth, 1997). Bakun (1999) considers the earthquake record complete for  $M \geq 5.5$  back to 1850. He notes that little is known about SFBR seismicity prior to that date, although he lists four earthquakes, three with estimated magnitudes of 6.0–6.5 and the fourth and largest (the 1838  $M$  6.8 earthquake) between 1836 and 1850 (Bakun, 1999, his table 2). Prior to 1836, Townley and Allen (1939) report at least seven felt earthquakes in the SFBR between October 1800 and September 1829. From May 1851 through April 1903, Bakun (1999) lists 55 earthquakes in the 4.6–6.4 magnitude range. Of these, 44 are estimated to have been  $M \geq 5.5$ . The magnitudes noted here are mean values from the analysis of Bakun (1999), and the uncertainties can be large. It is difficult to identify the sources of most of the preinstrumental seismicity. Wesson *et al.* (2003) applied Bayesian inference to associate the preinstrumental earthquakes with specific faults. They conclude that while reasonable probabilities of an association can be made for some of the larger earthquakes, the sources of most of the events in the Bakun (1999) catalog are uncertain.

In their overview of the effects of pre-1900 earthquakes throughout California, Topozada *et al.* (1981) conclude that by 1800 the record of earthquakes within 100 km of the coast between San Diego and Sonoma is probably complete for earthquakes of  $M \sim 7$  or larger. The founding of the Mission Dolores and the Presidio in San Francisco in 1776 provides an

important point in time for evaluating the occurrence of large SFBR earthquakes. Mission Dolores was the first of six Franciscan missions constructed along the length of the Bay Area between San Juan Bautista (1797) and Sonoma (1827). The missions are known to have kept records of felt earthquakes and earthquake damage. In their research and review of the 1836 and 1838 earthquakes, Topozada and Borchardt (1998) found no historical evidence of the occurrence of any large SFBR earthquakes between the founding of the Mission Dolores and 1838. The earliest earthquakes listed for the SFBR (Townley and Allen, 1939) occurred 11 October through 31 October 1800. They were felt in San Juan Bautista (sometimes six in a day), buildings were damaged, and ground cracks were reported near rivers. Therefore, 1776 has become the accepted date for the beginning of the historical period for large ( $M \sim 7$  or larger) earthquakes in the SFBR and has been used in a series of studies (i.e., Hecker *et al.*, 2005; Hall and Niemi, 2008; Kelson *et al.*, 2008) to trim radiocarbon probability density functions (PDFs) in dating models of recent SFBR paleoearthquakes. There is probably some softness in this date, for although the Mission Dolores was founded in 1776, construction of the permanent mission building was started in 1782 and completed in 1791. Acknowledging this caveat, we continue to use 1776 as the beginning of the historical period for large earthquakes and a cap for radiocarbon dating of post-1600 paleoearthquakes.

Prior to the historical record, the basis for the occurrence and timing of large (surface faulting) Bay Area earthquakes is paleoseismology. The length of the record and its completeness vary for each fault. However, the timing of the most recent surface rupture is available for the principal faults that have not broken historically (Rodgers Creek, northern section of the Hayward, northern Calaveras, San Gregorio, Concord–Green Valley). Dates of the penultimate rupture also have been developed at locations along the 1906 rupture trace of the San Andreas fault and on the 1868 Hayward fault rupture. There are no paleoearthquake dates for the Greenville fault, the Mt. Diablo blind thrust, or the northern extension of the Concord–Green Valley fault. With the exceptions noted here, the overall paleoseismic record appears to be complete back to about 1600. It is on this basis that we start our regional clock at this date.

## Surface-Faulting Earthquakes since 1600

### Dating the Recent Surface Ruptures

Fault ruptures that produce large moment-releasing earthquakes typically leave their signature at the surface. This is recorded in the stratigraphy exposed in trenches excavated across the faults. Paleoearthquake dates for the SFBR primarily rely on the use of radiocarbon dating, with the most commonly available organic material being detrital charcoal. A single sample provides a mean age of the sample and a counting uncertainty. This, in turn, is dendrochronologically calendar corrected to provide the full possible age range of the

Table 2  
Summary of Dates of SFBR Post-1600 Paleoearthquake Surface Ruptures

Paleoseismic Site*	Fault/Segment†	2 $\sigma$ Age Range (A.D.) of Surface Rupture‡	Date (A.D.) of Surface Rupture§	Reference
Filoli	SAP	$\geq 1450$ –1670	1600 <sup>  </sup>	Hall <i>et al.</i> (1999)
Lopes Ranch	CGV	1511–1725	1610	Lienkaemper <i>et al.</i> (2013)
Arano Flat Grizzly Flats	SAS	1584–1659	1624	Fumal, Dawson, <i>et al.</i> , 2004; Fumal, Heingartner, Samrad, <i>et al.</i> , 2004; T. Fumal, written comm., 2010)
Tyson's Lagoon	HS	1537–1737	1629	Schwartz <i>et al.</i> (1998)
Mira Vista	HN	1635–1776	1705	Lienkaemper <i>et al.</i> (2002)
Tyson's Lagoon	HS	1658–1786	1725	Lienkaemper and Williams (2007)
Fort Ross Orchard	SAN	1660–1812	1735 <sup>  </sup>	Hayward Fault Paleoearthquake Group (1999)
Vedanta Marsh	SAN	1680–1790		Lienkaemper <i>et al.</i> (2002)
Vedanta Marsh	SAN	1680–1740		Lienkaemper and Williams (2007)
Dogtown	SAN	1695–1776		Kelson <i>et al.</i> (2006)
Offshore	SAN + SAO	1700–1750		Niemi <i>et al.</i> (2004)
North Foothill	CN	1692–1776	1740	Zhang (2005)
Triangle G	RC	1690–1776	1745	Zhang <i>et al.</i> (2006)
Mill Canyon	SJB	1711–1770	1750	Hall and Niemi (2008)
Pillar Point Marsh	SG	1700–1776	1759	Goldfinger <i>et al.</i> (2007, 2008)

\*Site locations are shown in Figure 2.

†Fault segment to which surface rupture is assigned (Table 1).

‡2 $\sigma$  age range of rupture per reference.

§Mean event age from OxCal model as per reference unless noted otherwise.

||Mean age selected in present study (see text and Appendix A).

sample, which is represented by a PDF. The ideal field situation is the occurrence of datable deposits immediately below and above a rupture event horizon, but even here the uncertainties in the age ranges of these units can be broad. By using radiocarbon PDFs for each horizon, the probability distribution can be trimmed and reweighted using a radiocarbon calibration program such as OxCal (Bronk Ramsey, 2001, 2007; Lienkaemper and Bronk Ramsey, 2009). The result, generally, is a tighter distribution from which a mean date of the event and 1 $\sigma$  and 2 $\sigma$  uncertainty ranges can be extracted. For radiocarbon samples formed in the seventeenth and eighteenth centuries, the age-range probabilities can extend well into the nineteenth and/or twentieth centuries. This is a potential problem for estimating the ages of the relatively recent paleoearthquakes considered here, particularly where a rupture offsets a dated horizon and there is no unfaulted overlying deposit or the postevent deposit is not datable. For this reason, the historical record provides a major time constraint that allows radiocarbon PDFs to be truncated at 1776.

In addition to radiocarbon, the presence or absence of non-native pollen (Mensing and Byrne, 1998; Reidy, 2001) has provided a basis for event dating at some locations. Of particular importance is non-native *Erodium* pollen, which first appeared in the SFBR about 1770 and was ubiquitous in the region by 1800. The presence or absence of this pollen in critical deposits plays an important role in dating SFBR

paleoearthquakes that occurred between the mid–late 1700s and early–middle 1800s.

#### Timing of Paleoearthquakes

The paleoearthquakes (pre-1776) used in our analysis are listed in Table 2 and briefly summarized here. A detailed compilation of the reported observations and interpretations at locations in the SFBR that are used to develop the chronology of post-1600 surface ruptures is presented in Appendix A. It describes event ages and their uncertainties, including those associated with radiocarbon and other dating issues, and alternative stratigraphic and structural interpretations.

Table 2 lists the sites (Fig. 2) for which dates have been obtained and the fault segment with which each site is associated. With the exception of the Peninsula and Offshore segments of the San Andreas fault, each site provides direct exposure of the dated surface rupture. The Peninsula event is inferred from the geometry of buried stream channels at the Filoli site (Hall *et al.*, 1999), and the Offshore chronology is based on correlation and dating of turbidites (Goldfinger *et al.*, 2007, 2008). The two columns of age dates have important differences. The date of surface rupture column in Table 2 contains a single value. For all but the North Coast San Andreas, the listed date is the mean date of the event derived statistically from an OxCal model and reported by each investigator (Appendix A). The North Coast San Andreas has multiple

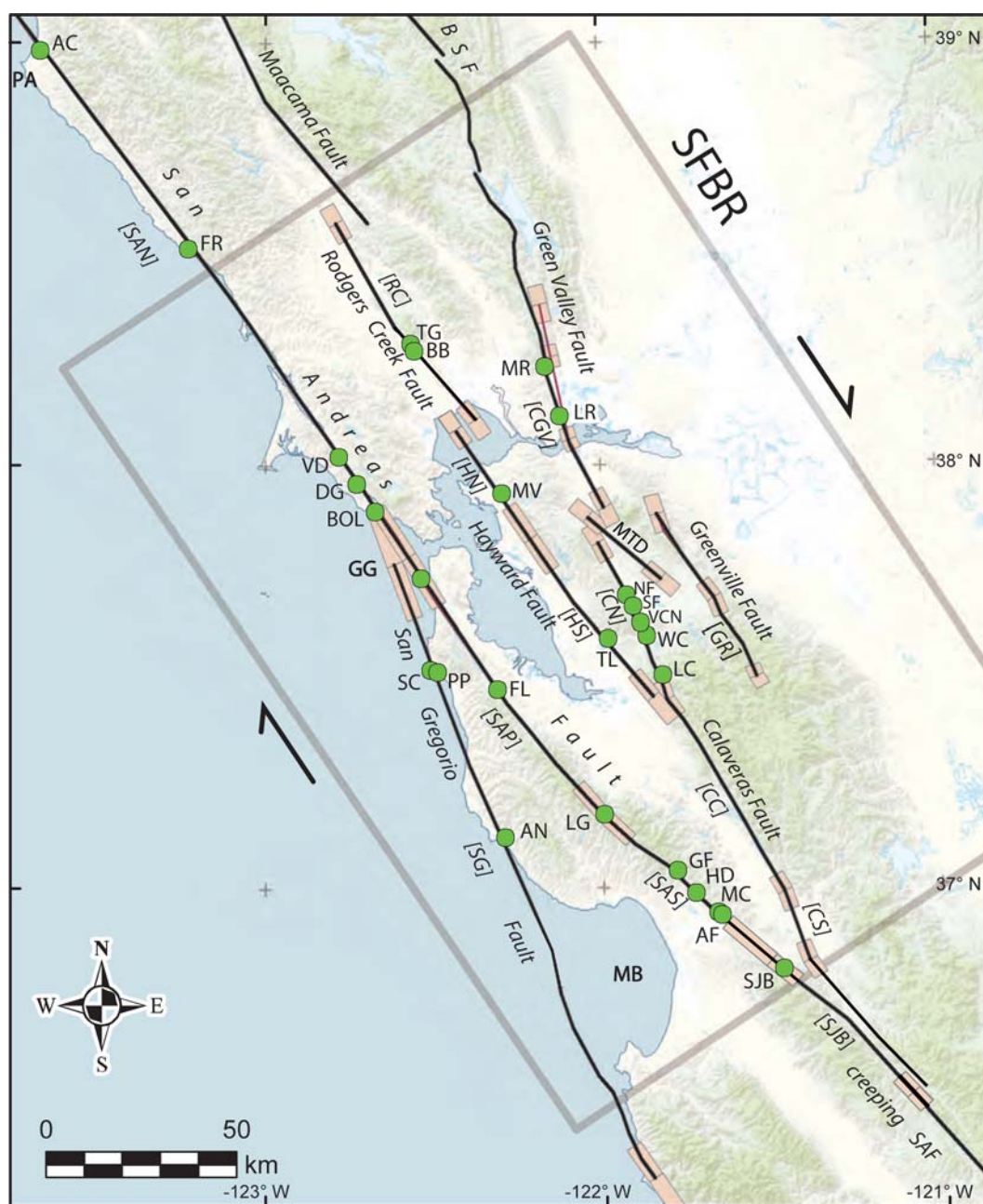


**Figure 2.** Paleoseismic site locations and other localities referred to in the text. Fault segmentation is the same as in Figure 1 but shown in greater detail. Solid-color rectangles are fault segment boundaries. The horizontal line within each boundary is the preferred rupture segment endpoint for determining fault rupture length, but rectangle length indicates overall uncertainty in endpoint location. Paleoseismic sites and other locations are as follows: NF, North Foothill; SF, South Foothill; AC, Alder Creek; FR, Fort Ross Orchard; VD, Vedanta Marsh; DG, Dogtown; BOL, Bolinas Lagoon; SC, Shelter Cove; PP, Pillar Point Marsh; AN, Ano Nuevo; FL, Filoli; LG, Los Gatos; GF, Grizzly Flats; HD, Hazel Dell; MC, Mill Canyon; AF, Arano Flat; SJB, San Juan Bautista; TG, Triangle G; BB, Beebe Ranch; MV, Mira Vista; TL, Tyson's Lagoon; MR, Mason Road; LR, Lopes Ranch; VCN, Valley Crest Nursery; WC, Welch Creek; LC, Leyden Creek; BSF, Bartlett Springs fault; PA, Point Arena; GG, Golden Gate; and MB, Monterey Bay.

penultimate event dates from both land and offshore sites, and we have arbitrarily set the event date at the midpoint of the  $2\sigma$  age ranges. The mean dates are regarded as the placeholders for each event and are used in the figures and tables that follow. Although they may reasonably approximate the actual date of each rupture, they are free to be moved about within

the more robustly constraining  $2\sigma$  age range. The  $2\sigma$  age range of surface rupture column in Table 2 lists the OxCal-derived age range for each. The event must postdate the oldest date in the range. The upper bound of this range is derived either directly from the dating or from the historical constraints discussed previously in this paper.

Between 1635 and the founding of the Mission Dolores (1776), ruptures occurred on the Hayward fault (north and south segments), San Andreas fault (North Coast and likely Offshore, and the San Juan Bautista segment), northern Calaveras fault, Rodgers Creek fault, and San Gregorio fault. It is likely that these were post-1658 if the northern and southern Hayward segments failed together, and they may have all occurred after 1690. Prior to 1635, we list ruptures on the Hayward (south), San Andreas (Santa Cruz mountains and Peninsula segments), and Concord–Green Valley faults. Within the  $2\sigma$  uncertainty, the true age of each event could predate 1600, although their mean dates place them in the early 1600s. Also listed is a San Andreas Peninsula event, for which occurrence is permissive although poorly constrained (Appendix A).

### Multiple Segment Ruptures

Examination of the  $2\sigma$  age ranges shows the timing of the most recent event at the Triangle G site on the Rodgers Creek fault overlaps the timing of the most recent event at the Mira Vista site on the northern Hayward fault and the penultimate event on the southern Hayward at Tyson’s Lagoon. This allows the possibility that both faults, or sections of both faults, could have ruptured together. Alternative rupture scenarios for the Hayward and Rodgers Creek faults have been previously described (WGCEP, 2003; Hecker *et al.*, 2005) and incorporated into the estimates of SFBR earthquake probability (WGCEP, 2003, 2008).

The dates of the penultimate rupture on the North Coast San Andreas segment (from multiple sites) and the San Gregorio fault at Pillar Point Marsh overlap (Table 2). The intersection geometry of these faults is similar to that of the intersection of the Denali and Totschunda faults in Alaska (Schwartz *et al.*, 2012), where the 2002 rupture of the  $M_w$  7.9 Denali fault earthquake propagated from the central Denali fault onto the Totschunda fault (Haeussler *et al.*, 2004). Schwartz *et al.* (2012) entertain the possibility that the San Andreas and San Gregorio faults ruptured together. Based on the combination of intersection geometry and paleoearthquake dates, we include a scenario in which the North Coast San Andreas and San Gregorio faults failed together in the post-1600 period. Goldfinger *et al.* (2007, 2008) interpret the distribution of turbidites offshore of the northern San Andreas fault as evidence of rupture between the Mendocino triple junction and the Golden Gate, which would include the North Coast and Offshore segments of the San Andreas (Fig. 1). In this case, a combined rupture of the San Andreas and San Gregorio faults is a multifault rupture scenario that is comparable in length to that of 1906. The uncertainty associated with the occurrence of a mid-1600s Peninsula segment rupture has been noted. Even so, we allow the possibility that if it occurred, it could have failed along with the Santa Cruz mountains segment. These alternative rupture scenarios are used in the construction of the alternative SFBR paleoearthquake sequences (Figs. 3 and 4, Table 3).

### Magnitudes of Post-1600 Earthquakes

The observations at each SFBR paleoseismic site show that a fault ruptured the surface at some datable time in the past. The question is, what magnitude earthquakes do these ruptures represent? Estimating the magnitude of paleoearthquakes is a challenge, but there are types of observations and analysis from which estimates can be developed. These include (1) the amount of coseismic surface offset associated with a paleorupture, measured directly from offset channels exposed in fault-parallel trenches (for strike-slip faults) or from associated geomorphic features, and the amount of average slip calculated from a fault slip rate and recurrence interval (RI) and (2) the use of scaling relations between magnitude and static fault parameters such as fault area. Through a series of field observations and statistical relations, we show that the post-1600 paleoearthquake ruptures described from the SFBR trenches are indicative of large slip per event (Appendix B) and that we can make reasonable estimates of the magnitude they represent.

### Observed Paleo Offsets

The inventory of measured coseismic surface offsets for both paleoruptures and historical ruptures on SFBR faults is small, with only a limited number of post-1600 measurements (Table 4, Appendix B). These have been made on the northern San Andreas at Alder Creek, the San Gregorio fault at Seal Cove, the Rodgers Creek fault at the Beebe Ranch and Triangle G sites, and the Hayward fault at Tyson’s Lagoon (Fig. 2). A geodetic estimate of average slip has been modeled for the 1868 Hayward fault rupture (Yu and Segall, 1996); although not paleoseismic, it is the single estimate of right lateral coseismic offset along the fault.

For long surface ruptures, the amount of slip typically varies along strike. With only one or at most a couple of measurements along a fault, the question is open as to whether the observed offset represents the average or a value much greater or less than the average. The maximum slip is generally limited to a short section of a rupture (see reviews of fault slip distributions by Hemphill-Haley and Weldon, 1999; Manighetti *et al.*, 2005; Wesnousky, 2008; Hecker *et al.*, 2010), and the likelihood of having sampled it at one of the SFBR paleoseismic localities is small. Similarly, the minimum slip generally occurs at the ends of a rupture, and the offset locations listed in Table 4 are not close to fault segment endpoints (Fig. 2). Hemphill-Haley and Weldon (1999) look at the relation between the number of sampling sites and the slip distribution for surface ruptures. They conclude the mean slip for a small number of measurement locations overestimates the actual mean for an entire rupture by 10%–20%, which is a small difference. We suggest the SFBR field measurements are more likely to approach average slip values for the respective paleoearthquakes. Note from Table 4 that the paleoseismically and/or historically measured slip at a point is, within a factor of two, the amount of average slip per event calculated from slip rate and recurrence interval.

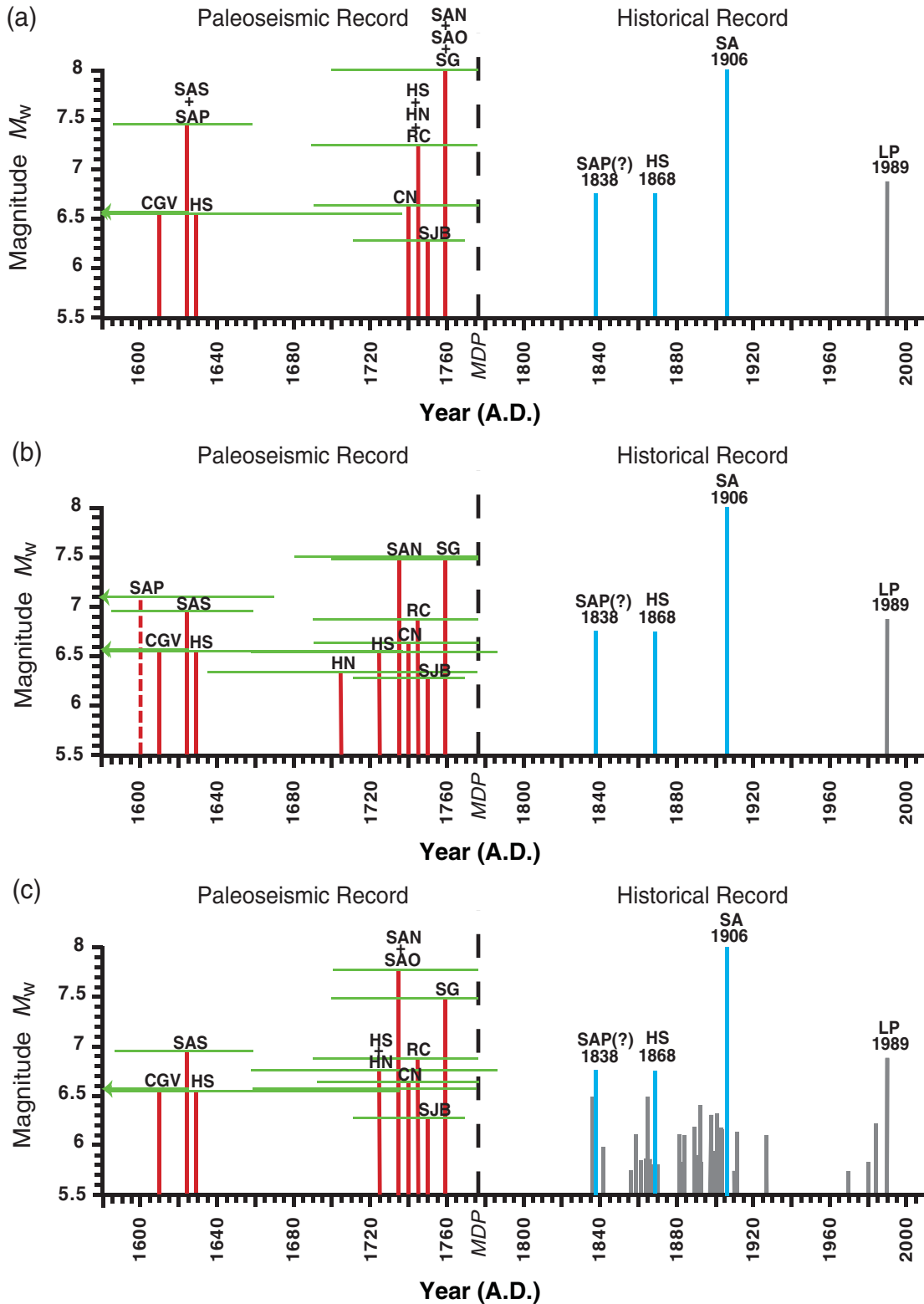


**Figure 3.** SFBR earthquake history, 1600–2010, showing alternative rupture source sequences. The vertical red lines are the mean dates (Table 3, Appendix A) and calculated mean magnitudes (Table 5) of each paleoearthquake. The horizontal green lines are  $2\sigma$  radiocarbon uncertainties; an arrow at the left end indicates an older part of age range extends beyond 1580. The vertical blue lines are dates and magnitudes of historical surface ruptures. The vertical gray lines are moderate magnitude historical earthquakes (Bakun, 1999). LP, 1989  $M$  6.9 Loma Prieta earthquake; MDP, initial construction of Mission Dolores and the Presidio (1776). (a) Minimum source model ( $S_{min}$ ) contains multisegment ruptures and the fewest number of 1600–1776 earthquake sources; (b) maximum source model ( $S_{max}$ ) contains only independent rupture segments and the largest number of earthquake sources. The dashed vertical red line for Peninsula San Andreas (SAP) reflects the uncertainty as to whether it did or did not occur during this time frame; and (c) intermediate source model ( $S_{int}$ ), which is the preferred model in this analysis.

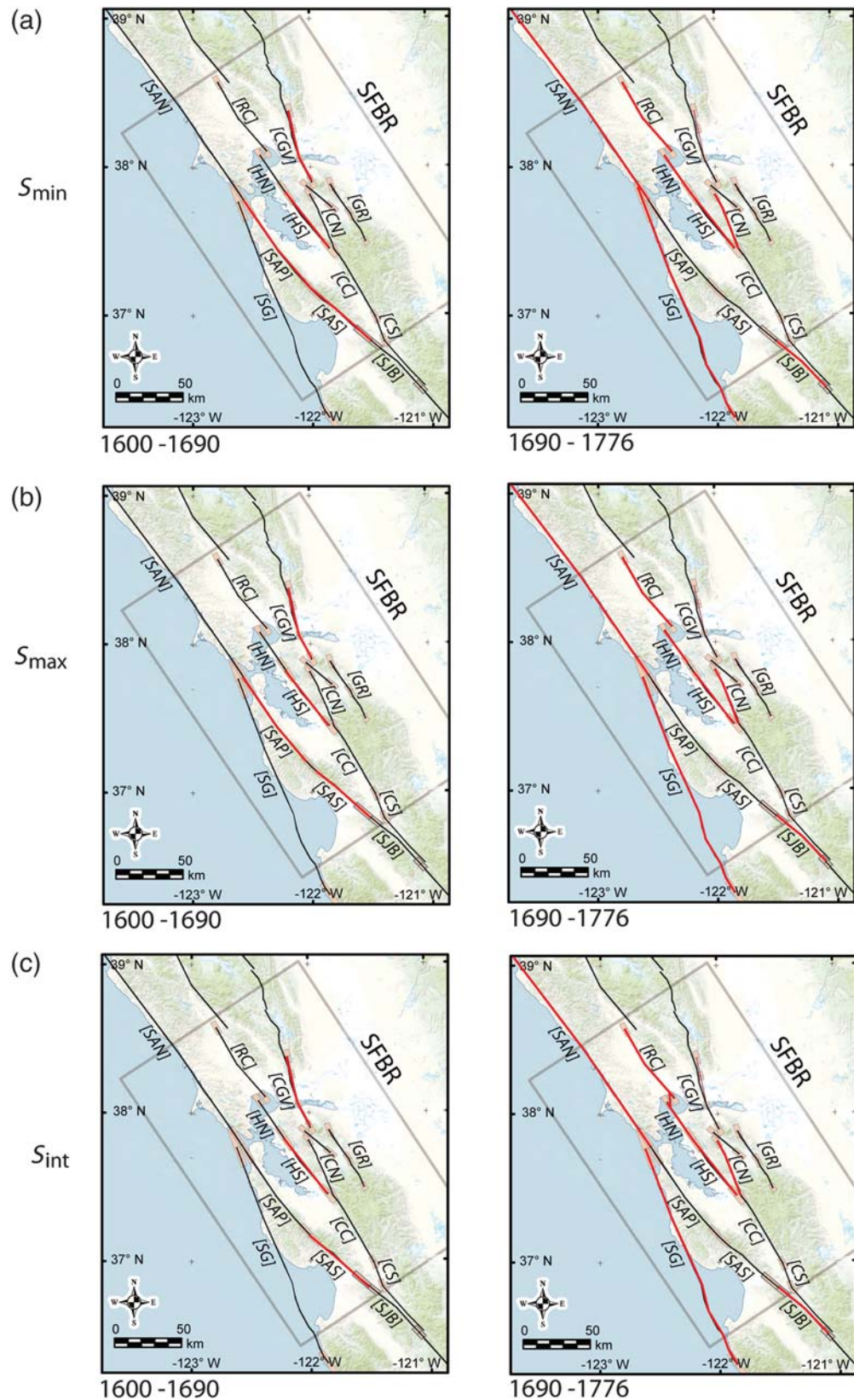


**Figure 4.** Maps of proposed paleoseismic surface ruptures for the 1660–1776 time interval: (a) minimum source model,  $S_{\min}$ ; (b) maximum source model,  $S_{\max}$ ; and (c) preferred source model,  $S_{\text{int}}$ . These reflect the rupture chronologies listed in Table 3 and the paleoearthquakes shown in Figure 3. There are no data on timing of the most recent surface rupture on the Greenville (GR) fault or the northern extension of the Concord–Green Valley (CGV) fault. The central Calaveras (CC) fault is creeping at or near its long-term plate rate, and it is uncertain whether it produces large surface ruptures; none has been interpreted for the paleoseismic time interval of interest here.

Table 3  
SFBR Rupture Source Sequences

Minimum Rupture Source ( $S_{\min}$ )*	Event Age <sup>†</sup>	Maximum Rupture Source ( $S_{\max}$ )*	Event Age <sup>†</sup>	Intermediate Rupture Source ( $S_{\text{int}}$ )*	Event Age*
CGV	1511–1625 (1610)	SAP	≥1450–1670 (1600)	CGV	1511–1625 (1610)
SAS + SAP	1585–1659 (1624)	CGV	1511–1625 (1610)	SAS	1585–1659 (1624)
HS	1537–1737 (1629)	SAS	1585–1659 (1624)	HS	1537–1737 (1629)
CN	1692–1776 (1740)	HS	1537–1737 (1629)	HN + HS	1658–1786 (1725)
RC + HN + HS	1690–1776 (1745)	HN	1635–1776 (1705)	SAO + SAN	1700–1776 (1735)
SJB	1711–1770 (1750)	HS	1658–1786 (1725)	CN	1692–1776 (1740)
SAO + SAN + SG	1700–1776 (1759)	SAN	1680–1776 (1735)	RC	1690–1776 (1745)
		CN	1692–1776 (1740)	SJB	1711–1770 (1750)
		RC	1690–1776 (1745)	SG	1700–1776 (1759)
		SJB	1711–1770 (1750)		
		SG	1700–1776 (1759)		

Three models that bracket the range of rupture sources are shown. These are the minimum source model ( $S_{\min}$ ), which contains multisegment ruptures and the fewest number of 1600–1776 earthquake sources; the maximum source model ( $S_{\max}$ ), which contains all independent and the largest number of earthquake sources; and ( $S_{\text{int}}$ ), which is the preferred source model.

\*Fault and fault segment names as listed in Table 1.

<sup>†</sup>Event age is shown as  $2\sigma$  range and mean date. Where multiple fault segments comprise a rupture source, the best-constrained segment date (italics) is used for the mean event age. These source sequences are plotted graphically in Figure 3.

#### Average Slip from Slip Rate and Recurrence Interval

Slip rates for SFBR faults listed in Table 4 were developed by the WGCEP (2003) as consensus rates. They are primarily based on geologic offsets and represent rates averaged over several hundred to several thousand years. Creep rates play a major role in estimating the slip rate for the central Calaveras fault and to a lesser degree the slip rates on the Concord–Green Valley and Hayward faults. d’Alessio *et al.* (2005) developed slip rates from a geodetic block model for the SFBR. These are in general agreement with the geologic rates on Table 4, although the preferred geodetic rates (d’Alessio *et al.*, 2005) are somewhat higher for the Greenville fault (5.6 mm/yr) and Concord–Green Valley fault (6.7–7 mm/yr) and lower for the San Gregorio fault (2.5 mm/yr). Recurrence interval estimates listed in Table 4 are (a) calculated from the SFBR fault model by WGCEP (2003, their table 4.9) and (b) a subset of SFBR faults for which there is paleoseismic information (appendix B of WGCEP, 2008). Table 4 lists these geologic slip rates and recurrence intervals, as well as the slip per event that we have calculated from these parameters. The average slip per event anywhere along the SFBR fault system is larger than 1 m.

Wells and Copper-Smith (1994) developed a series of regressions relating moment magnitude to a range of fault parameters. One of these is the relation between average displacement and magnitude:

$$M = a + b \times \log(AD), \quad (1)$$

in which  $a$  and  $b$  are coefficients and  $AD$  is the average displacement. For strike-slip faults, the value of  $a$  is 7.04 ( $\pm 0.05$ ) and  $b$  is 0.89 ( $\pm 0.09$ ). Using the calculated mean average slip per event (Table 3) and the Wells and Copper-Smith (1994) regression, the minimum calculated mean moment magnitude for the fault system is  $M$  7, which is on

the Concord–Green Valley fault. Although this indicates that the paleoearthquakes we are concerned with are large, the magnitude developed using only average slip lacks the precision we require and, at least for the creeping faults, likely overestimates it.

#### Magnitude Estimates from Fault Area

To estimate the magnitudes of paleoearthquakes in the 1600–1776 interval, we use the relation between fault area and moment magnitude, which requires information on fault rupture length and width. We rely heavily on the WGCEP (2003) model of the SFBR fault system that includes estimates of fault rupture lengths, down-dip fault widths, and the effects of creep on earthquake magnitude. (See Data and Resources for online access to the full WGCEP, 2003, report, or to specific chapters of the report; chapter 3, Characterization the SFBR Rupture Sources, provides details of the SFBR fault segmentation modeling, and chapter 4, The SFBR Earthquake Source Model: Magnitudes and Long-Term Rates, addresses the model itself.)

The basic building blocks for modeling SFBR fault ruptures are fault segments. These are faults or sections of faults that are considered capable of failing independently to produce an earthquake (e.g., the 1868 rupture of the southern part of Hayward fault) or that can join in multisegment ruptures, such as occurred in 1906. The fault segments and the boundary zones between segments are shown in Figures 1 and 2. These are derived from behavioral and kinematic observations. The behavioral considerations provide the strongest basis for segmentation, with the difference in timing of events on adjacent parts of a fault, either from paleoseismic observations or from the extent of historical surface rupture, being primary. For example, the estimated extent of the 1868 Hayward rupture (Yu and Segall, 1996)

Table 4  
Calculated and Observed Individual Event Slip for SFBR Faults

Fault/Segment*	Slip Rate (mm/yr) <sup>†</sup>	RI (yr) <sup>‡</sup>	Slip (m) <sup>§</sup>	RI (yr) <sup>  </sup>	Slip (m) <sup>#</sup>	RI (yr)**	Slip (m) <sup>††</sup>	Slip Measured (m) <sup>§§</sup>
SAN	24 (21–27)	223	5.35	248	5.95	248 (Zhang, 2005)	5.95	4.9 (1906) (Baldwin <i>et al.</i> , 2000); AC 3.1–4.6 (pen) (Baldwin <i>et al.</i> , 2000); AC
HS	9 (7–11)	161	1.44	170	1.53	161 (Lienkaemper <i>et al.</i> , 2010)	1.44	1.9 (± 0.4) (1868 geodetic) (Yu and Segall, 1996)
HN	9 (7–11)	155	1.39	—	—	—	—	—
RC	9 (7–11)	205	1.84	305	2.74	—	—	2.0 (+0.3, –0.2) (mre) (Budding <i>et al.</i> , 1991); BB ≥ 2.1 (+1.2, –0.8) (mre) (Hecker <i>et al.</i> , 2005); TG 2.8–5.4 (pen + prepen) (Budding <i>et al.</i> , 1991); BB
SG	7 (4–10)	392	2.74	—	—	—	—	5(+6, –2) (mre) (Simpson <i>et al.</i> , 1997); SC 3 (± 0.2) (pen) (Simpson <i>et al.</i> , 1997); SC
CN	6 (4–8)	187	1.12	465	2.79	—	—	—
CGV	5 (2–8)	210	1.05	—	—	220 Lienkaemper <i>et al.</i> (2013)	1.10	—

\*Abbreviations from Table 1.

<sup>†</sup>Mean slip rate (mm/yr) with 95% bounds (WGCEP, 2003, their table 3.8).

<sup>‡</sup>Mean recurrence interval (RI), calculated (WGCEP, 2003, their table 4.9).

<sup>§</sup>Mean slip (m) calculated from <sup>†</sup> and <sup>‡</sup>.

<sup>||</sup>Mean recurrence interval, paleoseismic (WGCEP, 2008, their appendix B).

<sup>#</sup>Mean slip calculated from <sup>†</sup> and <sup>\*\*</sup>.

<sup>\*\*</sup>Site-specific mean recurrence interval as per reference.

<sup>††</sup>Mean slip calculated from <sup>†</sup> and <sup>\*\*</sup>.

<sup>§§</sup>Measured site-specific slip for most recent event (mre) and penultimate surface rupture (pen); site locations (e.g., AC, TG) shown in Figure 2.

combined with differences in timing of post-1600 surface ruptures (Table 2, Appendix A) resulted in the division of the Hayward fault into northern and southern rupture segments. Locations of changes in slip rate (common at fault branches), the transition from locked to creeping sections of a fault or changes in the rate of creep along a fault, and the distribution of microearthquake activity provide additional bases for segmentation. Kinematic considerations are related to aspects of fault geometry that could affect rupture propagation. These include changes in strike, bends, and steps (the 5 km wide right step between the Rodgers Creek and Hayward fault is a principal basis for that boundary), branching or intersection points, changes in fault trace complexity, and variation in lithology along a fault. WGCEP (2003) recognized that ruptures may not stop at preferred segment end points, hence it defined zones of uncertainty based on the range of available observations (Fig. 2). In contrast to WGCEP (2008), which defined specific segment endpoints with no uncertainty, the WGCEP (2003) segmentation model provides mean, maximum, and minimum fault rupture lengths (WGCEP, 2003, their table 3.8).

The present analysis modifies the WGCEP segmentation model slightly. It treats the San Gregorio fault as a single structure (SG in Figs. 1 and 2, Table 1) because there was

little basis for a segment boundary in Monterey Bay. It also redefines the southern end of the Santa Cruz Mountains segment as the San Juan Bautista segment (Appendix A), following Johanson and Burgmann (2005), who conclude it is a distinct transition zone into the fully creeping section of the San Andreas fault. With these modifications, the WGCEP (2003) fault segment lengths are used in our calculation of fault area.

WGCEP (2003) estimated fault widths and their uncertainties (their table 3.8) based on the depth distribution of seismicity along each fault and a regional heat flow model. Rather than a single rupture width for all sources, the fault-specific width varies based on these observations. The average depth of seismicity in the SFBR is 11–12 km and locally extends to 15–16 km. The areas of deepest seismicity, such as the Santa Cruz Mountains and Mt. Diablo, are regions of transpression in the strike-slip fault system with thickened brittle crust.

Creep occurs on some faults in the SFBR, including the Hayward, Concord–Green Valley, Northern Calaveras, and the northern section of the Rodgers Creek. To account for it, a seismogenic-scaling factor,  $R$ , was developed (WGCEP, 2003, their table 3.8), which uses measured or estimated creep rates for each fault and has the effect of reducing

Table 5  
Estimates of Moment Magnitude ( $M_w$ ) and Seismic Moment ( $M_0$ ) for SFBR Earthquake Rupture Sources

Earthquake Rupture*	Seismogenic Area Mean <sup>†</sup> (km <sup>2</sup> )	Area Maximum (km <sup>2</sup> )	Area Minimum (km <sup>2</sup> )	$M_w$ Mean <sup>‡</sup>	$M_w$ Maximum	$M_w$ Minimum	$M_0$ Mean (10 <sup>E</sup> dyn·cm) <sup>§</sup>	$M_0$ Maximum (dyn·cm)	$M_0$ Minimum (dyn·cm)
HN	235	391	119	6.35	6.57	6.06	3.77 <sup>25</sup>	8.10 <sup>25</sup>	1.36 <sup>25</sup>
HS	367	599	210	6.54	6.77	6.30	7.36 <sup>25</sup>	1.62 <sup>26</sup>	3.19 <sup>25</sup>
HN + HS	616	882	400	6.79	7.00	6.54	1.71 <sup>26</sup>	3.52 <sup>26</sup>	7.23 <sup>25</sup>
RC	736	949	563	6.89	7.04	6.74	2.45 <sup>26</sup>	4.07 <sup>26</sup>	1.43 <sup>26</sup>
HS + HN + RC	1359	1737	1044	7.25	7.39	7.09	8.35 <sup>26</sup>	1.36 <sup>27</sup>	4.92 <sup>26</sup>
SAN + SAO	3482	4432	2755	7.79	7.93	7.66	5.48 <sup>27</sup>	8.88 <sup>27</sup>	3.43 <sup>27</sup>
SAN	2042	2678	1545	7.48	7.64	7.32	1.88 <sup>27</sup>	3.24 <sup>27</sup>	1.08 <sup>27</sup>
SAN SFBR	1001	1306	757	7.07	7.22	6.91	4.53 <sup>26</sup>	7.71 <sup>26</sup>	2.59 <sup>26</sup>
SAP	1066	1483	765	7.11	7.30	6.91	5.13 <sup>26</sup>	9.94 <sup>26</sup>	2.64 <sup>26</sup>
SAS	829	1141	606	6.96	7.15	6.78	3.11 <sup>26</sup>	5.88 <sup>26</sup>	1.66 <sup>26</sup>
SAS + SAP	1907	2412	1483	7.44	7.58	7.30	1.64 <sup>27</sup>	2.63 <sup>27</sup>	9.94 <sup>26</sup>
SJB	202	332	97	6.29	6.50	5.97	3.01 <sup>25</sup>	6.33 <sup>25</sup>	9.77 <sup>24</sup>
SJB SFBR	88	130	54	5.92	6.09	5.71	8.64 <sup>24</sup>	1.55 <sup>25</sup>	1.00 <sup>25</sup>
1906 SFBR	2908	3718	2249	7.69	7.83	7.54	3.82 <sup>27</sup>	6.25 <sup>27</sup>	2.29 <sup>27</sup>
SG	1983	2513	1556	7.47	7.60	7.33	1.78 <sup>27</sup>	2.85 <sup>27</sup>	1.09 <sup>27</sup>
SG SFBR	1767	1995	1539	7.39	7.47	7.32	1.36 <sup>27</sup>	1.80 <sup>27</sup>	1.07 <sup>27</sup>
SG + SAN + SAO	5465	6945	4311	8.05	8.19	7.91	1.33 <sup>28</sup>	2.16 <sup>28</sup>	8.22 <sup>27</sup>
SG + SAN + SAO SFBR	2768	3301	2296	7.66	7.76	7.55	3.47 <sup>27</sup>	4.90 <sup>27</sup>	2.37 <sup>27</sup>
CGV	395	668	182	6.58	6.84	6.24	8.22 <sup>25</sup>	2.02 <sup>26</sup>	2.57 <sup>25</sup>
CN	465	610	348	6.65	6.78	6.52	1.05 <sup>26</sup>	1.68 <sup>26</sup>	6.80 <sup>25</sup>

\*Earthquake rupture sources; SFBR notation is for sections of sources that are in the SFBR rectangle but whose lengths extend beyond the boundaries. (See Table 1 for abbreviations.)

<sup>†</sup>Mean seismogenic area from [WGCEP \(2003\)](#); those with SFBR notation are calculated here. The mean is a preferred value ([WGCEP, 2003](#)) with width based on seismogenic crustal thickness from seismicity, length on best estimate of segment boundaries, and seismogenic scaling factor ( $R$ ) from creep. Variations in these parameters provide the maximum and minimum area, considered by [WGCEP \(2003\)](#) to be 2.5%–95% bounds.

<sup>‡</sup>Magnitude ( $M_w$ ) calculated using [Hanks and Bakun \(2008\)](#).

<sup>§</sup>Seismic moment ( $M_0$ ) calculated from the magnitude; mean is the preferred value.

the fault surface area available for rupture. This incorporates creep into the estimates of moment magnitude and moment release. Length, width, and  $R$  are combined to calculate the seismogenic area for each fault segment, including the mean and 95th percentile values ([WGCEP, 2003](#), their table 4.4). The mean is the preferred value based on the combined observations. The uncertainties are listed throughout the analysis that follows, but our calculations and interpretations rely principally on the mean (preferred) values.

Using the seismogenic rupture areas, we calculate the mean magnitude (with uncertainties) for each potential rupture source for the post-1600 paleoearthquakes. These are listed in Table 5. These magnitudes differ slightly from those calculated by [WGCEP \(2003](#), their table 4.4). That analysis uses and equally weights two distinct magnitude–area relations, those of Ellsworth in [WGCEP \(2003\)](#) and [Hanks and Bakun \(2002\)](#). The present analysis uses a single magnitude–area relation ([Hanks and Bakun, 2002, 2008](#)) to calculate the paleomagnitudes. The Hanks and Bakun relation is a bi-sloped curve with a change in slope at  $M$  6.71. Two equations give the magnitude for fault areas less than and greater than 537 km<sup>2</sup>:

$$M = \log A + 3.98 \pm 0.03(A \leq 537 \text{ km}^2) \quad (2)$$

and

$$M = 4/3 \log A + 3.07 \pm 0.04(A \geq 537 \text{ km}^2). \quad (3)$$

[Hanks and Bakun \(2002, 2008\)](#) is used in preference over [Wells and Coppersmith \(1994\)](#) because the latter underestimates the magnitude for larger fault areas. This is important when dealing with the longer rupture scenarios for the SFBR. From the estimates of magnitude, the moment for each can be calculated from the relation

$$M = 2/3 \log M_0 - 10.7 \quad (4)$$

([Hanks and Kanamori, 1979](#)). Table 5 lists the mean, maximum, and minimum moment calculated for each potential rupture source. The seismic moment of each and moment sums for different time intervals during the post-1600 earthquake sequence (Table 6) are the basic inputs for discussing moment release over time and the SFBR earthquake cycle.

## Discussion

In the following sections, the data on the timing of past surface-faulting earthquakes, the estimates of moment magnitude for different paleoruptures, and the historical seismic record are combined to discuss the chronology and size of surface-faulting earthquakes in the SFBR since approximately 1600, seismic moment release during this interval, and the implications for the earthquake cycle.

Table 6  
Seismic Moment Sums ( $\Sigma M_0$ ) and Moment Release Rates ( $\Sigma M_0/\text{yr}$ ) for Different Time Intervals between 1600 and 2012

Interval	$\Sigma M_0$ ( $10^E$ dyn-cm)			$\Sigma M_0/\text{yr}$ ( $10^E$ dyn-cm/yr)		
	Mean	Max	Min	Mean	Max	Min
1600–1776 ( $S_{\min}$ )*	6.21 <sup>27</sup>	9.44 <sup>27</sup>	3.99 <sup>27</sup>	3.53 <sup>25</sup>	5.36 <sup>25</sup>	2.27 <sup>25</sup>
1600–1776 ( $S_{\text{int}}$ )*	2.81 <sup>27</sup>	4.47 <sup>27</sup>	1.84 <sup>27</sup>	1.60 <sup>25</sup>	2.54 <sup>25</sup>	1.05 <sup>25</sup>
1600–1776 ( $S_{\max}$ )*	3.26 <sup>27</sup>	5.35 <sup>27</sup>	2.08 <sup>27</sup>	1.85 <sup>25</sup>	3.04 <sup>25</sup>	1.18 <sup>25</sup>
1690–1776 ( $S_{\min}$ )*	4.42 <sup>27</sup>	6.44 <sup>27</sup>	2.93 <sup>27</sup>	5.14 <sup>25</sup>	7.49 <sup>25</sup>	3.41 <sup>25</sup>
1690–1776 ( $S_{\text{int}}$ )*	2.34 <sup>27</sup>	3.51 <sup>27</sup>	1.61 <sup>27</sup>	2.72 <sup>25</sup>	4.08 <sup>25</sup>	1.87 <sup>25</sup>
1690–1776 ( $S_{\max}$ )*	2.28 <sup>27</sup>	3.40 <sup>27</sup>	1.59 <sup>27</sup>	2.65 <sup>25</sup>	3.95 <sup>25</sup>	1.85 <sup>25</sup>
1600–1776 ( $S_{\min}$ ) <sup>†</sup>	6.87 <sup>27</sup>	1.11 <sup>28</sup>	4.64 <sup>27</sup>	3.90 <sup>25</sup>	6.31 <sup>25</sup>	2.64 <sup>25</sup>
1600–1776 ( $S_{\text{int}}$ ) <sup>†</sup>	3.47 <sup>27</sup>	6.14 <sup>27</sup>	2.49 <sup>27</sup>	1.97 <sup>25</sup>	3.49 <sup>25</sup>	1.42 <sup>25</sup>
1600–1776 ( $S_{\max}$ ) <sup>†</sup>	3.92 <sup>27</sup>	7.02 <sup>27</sup>	2.73 <sup>27</sup>	2.23 <sup>25</sup>	3.99 <sup>25</sup>	1.55 <sup>25</sup>
1777–1835 <sup>‡</sup>	8.64 <sup>25</sup>	1.22 <sup>26</sup>	5.57 <sup>25</sup>	1.49 <sup>24</sup>	2.10 <sup>24</sup>	9.60 <sup>23</sup>
1836–1905 <sup>§</sup>	5.87 <sup>26</sup>	1.16 <sup>27</sup>	2.96 <sup>26</sup>	8.51 <sup>24</sup>	1.68 <sup>25</sup>	4.29 <sup>24</sup>
1836–1905 <sup>  </sup>	1.09 <sup>27</sup>	2.83 <sup>27</sup>	9.49 <sup>26</sup>	1.58 <sup>25</sup>	4.10 <sup>25</sup>	1.37 <sup>25</sup>
1836–1905 <sup>#</sup>	6.56 <sup>26</sup>	1.67 <sup>27</sup>	6.53 <sup>26</sup>	9.51 <sup>24</sup>	2.42 <sup>25</sup>	9.46 <sup>24</sup>
1777–1905 <sup>§</sup>	5.87 <sup>26</sup>	1.16 <sup>27</sup>	2.96 <sup>26</sup>	4.59 <sup>24</sup>	9.06 <sup>24</sup>	2.31 <sup>24</sup>
1777–1905 <sup>§  </sup>	1.17 <sup>27</sup>	2.78 <sup>27</sup>	1.02 <sup>27</sup>	9.14 <sup>24</sup>	2.17 <sup>25</sup>	7.97 <sup>24</sup>
1906 <sup>  </sup>	2.85 <sup>27</sup>	5.09 <sup>27</sup>	1.73 <sup>27</sup>	–	–	–
1906 <sup>**</sup>	3.82 <sup>27</sup>	6.25 <sup>27</sup>	2.29 <sup>27</sup>	–	–	–
1906–1977 <sup>  </sup>	1.04 <sup>26</sup>	1.49 <sup>26</sup>	5.81 <sup>25</sup>	1.46 <sup>24</sup>	2.1 <sup>24</sup>	8.18 <sup>23</sup>
1977–1998 <sup>  ‡</sup>	2.97 <sup>26</sup>	8.27 <sup>26</sup>	2.34 <sup>26</sup>	1.40 <sup>25</sup>	3.93 <sup>25</sup>	1.11 <sup>25</sup>
1906–2012 <sup>††</sup>	2.51 <sup>26</sup>	–	–	2.38 <sup>24</sup>	–	–

\*Surface faulting only; derived from Tables 4 and 5.

<sup>†</sup>Combined surface faulting and seismicity estimate (see text).

<sup>‡</sup>Assumes same  $\Sigma M_0/\text{yr}$  of  $1.12 \times 10^{24}$  dyn-cm/yr for 58 years as calculated by Bakun (1999) for  $M \leq 5.5 + M \geq 5.5$  for 19 April 1906 to 1 January 1977, following the 1906 earthquake.

<sup>§</sup>Moment for 1838 and 1868 earthquakes only based on magnitudes from Bakun (1999).

<sup>||</sup>From table 3 of Bakun (1999).

<sup>#</sup>Moment for moderate earthquakes only during this interval.

\*\*1906 rupture within the SFBR, derived from WGCEP (2003) seismogenic area (Table 5).

<sup>††</sup>Only Loma Prieta in interval.

### SFBR Earthquake History since 1600

The development of a chronology of earthquakes for the past 400 years is confronted with a range of uncertainties and assumptions. For the paleoearthquakes, these include the timing of individual surface ruptures, the accuracy of fault segmentation models, the extrapolation of rupture timing at a point along a fault segment or a multisegment rupture, and estimates of fault area for calculating magnitude. For pre-instrumental historical earthquakes (Bakun, 1999), the sources and magnitudes are the primary uncertainties. We incorporate these as far as possible by constructing alternative models of the SFBR earthquake history, particularly for the 1600–1776 paleoseismic interval. Three models are presented (Figs. 3, 4, Table 3) that we consider to reasonably bracket paleoearthquake rupture behavior based on our interpretation of the available data (Appendix A). These are (1) a minimum source chronology ( $S_{\min}$ ) that contains the largest number of multisegment fault ruptures and the fewest paleoearthquakes (Figs. 3a, 4a), (2) a maximum source chronology ( $S_{\max}$ ) that contains only single segment ruptures and the largest number of events (Figs. 3b, 4b), and (3) an intermediate source chronology ( $S_{\text{int}}$ ) that is our preferred interpretation of the paleorupture history (Figs. 2c, 3c). For multiple

segment ruptures, the best-constrained date on the participating segments is the basis for both the  $2\sigma$  age range and the mean date (Table 3). Historical ruptures are added to Figure 3c, along with the year and mean magnitude of the moderated  $M \leq 5 + M \geq 5.5$  historical events (Bakun, 1999) to extend the earthquake history to 2012.

The most robust observation from the paleoseismic data is that in an interval of 176 years (1600–1776), the complete SFBR fault system essentially failed in a series of surface-faulting earthquakes that physically spanned the length of the SFBR rectangle (Fig. 4). The two major strike-slip faults in the region for which there are no surface-rupture timing data are the Greenville fault and the northern continuation of the Concord–Green Valley fault (Bartlett Springs fault). The sequences of individual paleoseismic events shown in Figure 3 reflect the mean dates developed in OxCal modeling of these ruptures (Tables 2 and 3, Appendix A). Given the  $2\sigma$  radiocarbon uncertainties, if one could shuffle and redeal this paleoseismic card deck, the actual sequences might have been quite different. Nonetheless, the paleoseismic analysis suggests that it was more likely that (a) the Concord–Green Valley fault, southern Hayward fault, and San Andreas fault (either as the Santa Cruz Mountains segment or as a combined rupture

with the Peninsula segment) produced earthquakes in the early part of the interval and (b) the majority of events (Hayward north and south, Rodgers Creek, northern Calaveras, San Andreas, and San Gregorio faults) occurred in the latter part of the interval. We interpret the more recent part of the sequence as a regional earthquake cluster.

Estimates of the duration of the cluster vary. The  $2\sigma$  radiocarbon age ranges permit a start date as early as 1635 if the northern Hayward ruptured as a separate segment (Table 2), yielding a maximum duration of 141 years. However, the cluster length was likely shorter. The North Coast San Andreas, southern Hayward, Rodgers Creek, northern Calaveras, San Gregorio, and San Juan Bautista ruptures occurred after 1658 (Table 2), giving a 118-year interval with the bulk of the probability density in the eighteenth century. If the southern and northern Hayward fault segments failed together, this would be a maximum interval (based on the southern Hayward age range). The Hayward event certainly could have occurred in the 1700s, and there are no other ruptures older than 1690. Additionally, the rupture sequence may have ended a decade or two prior to the construction of the Mission Dolores and Presidio. Although the duration of the cluster could have been as long as 118 years, it is more likely that the largest, if not all, of these paleoearthquakes occurred during a period of 100 years or less. For the purpose of calculating seismic moment rates, we have adopted a start date for the regional earthquake cluster of 1690.

From the end of the cluster until 1906, the SFBR was characterized by the infrequent occurrence of surface-faulting earthquakes on the major plate boundary faults. There appear to have been no large events for a minimum of 61 years (1776–1837), and there were only two during a minimum interval of 130 years (1776–1906). These were (1) the 1838 earthquake, the source of which (as noted previously) is uncertain, although attributed by many to the Peninsula San Andreas or more recently to the Santa Cruz mountains segment (Streig *et al.*, 2014), and (2) the 1868 Hayward fault earthquake. These ruptures occupy only a small percentage of the total length of the plate boundary fault system through the SFBR. As described by Bakun (1999) and illustrated in Figure 3c, other smaller earthquakes occurred throughout the region. The low frequency of occurrence of large earthquakes following the regional earthquake cluster is qualitatively similar to the absence of large earthquakes on principal SFBR faults during the 107 years (to date) following the 1906 event.

#### SFBR Moment Sums and Moment Release: 1600–2012

Earthquake recurrence also is viewed as moment release through time. One of our objectives is to quantify this release over the past approximately 400 years. Using the moment estimates from the regional earthquake sources (Table 5) and those from historical and instrumental seismicity (Bakun, 1999), we sum the moment ( $\Sigma M_0$ ) for different time intervals

and derive the moment rate per year ( $\Sigma M_0/\text{yr}$ ) (Table 6). In doing this, we have constructed two models that show estimates of the seismic moment distribution from 1600 to the present. One is based on estimates of moment for only the regional events associated with surface rupture (Fig. 5a). The 1989  $M_w$  6.9 Loma Prieta earthquake is the largest regional event since 1906 and contributes to SFBR moment release, but it did not rupture the surface and is not included in that plot. The second model combines paleoseismic and historical moment release (Fig. 5b). For each, we use the mean values of  $\Sigma M_0$  and  $\Sigma M_0/\text{yr}$ ; similar models can be constructed using both the maximum and minimum estimates of these values (Table 5).

*$\Sigma M_0/\text{yr}$  in Surface-Faulting Earthquakes.* The magnitude shown for each paleoearthquake in Figure 3 is for the full rupture of that source. The 1906 rupture involved all segments of the San Andreas fault between the Mendocino triple junction and San Juan Bautista, and the ~1735 northern San Andreas event likely involved both the North Coast and Offshore segments (Appendix A). These extend beyond the boundaries of the SFBR, as do full ruptures of the San Juan Bautista segment of the San Andreas fault and the San Gregorio fault (Figs. 1, 4). However, our interest is with the amount of moment released in the SFBR crust. Therefore, only the southern 90 km of the North Coast segment and the northern 20 km of the San Juan Bautista segment are used for ruptures involving those sources. The San Gregorio fault has been shortened by 25 km to reflect rupture within the SFBR. These changes to the area of the San Juan Bautista segment and San Gregorio have minor impact on overall moment release. The magnitudes and moments calculated for these shortened sources are listed in Table 5 with the designation SFBR.

The largest single contributor to moment release in the SFBR in the past 400 years is the 1906 earthquake. Estimates of its magnitude and of the moment released in the SFBR during that earthquake vary considerably. The seismic model of Wald *et al.* (1993) and the geodetic model of Thatcher *et al.* (1997) provide magnitudes of  $M_s$  7.7 and  $M_w$  7.9, respectively, with the seismic model yielding little information on the slip offshore northwest of Point Arena. Song *et al.* (2008) use triangulation data employing new projection methods that both confirm and refine previous geodetic analysis of the rupture (Thatcher *et al.*, 1997), and particularly offshore of Point Arena. Their final slip model, which uses a fault width of 12 km, gives a moment of  $7.9 \times 10^{27}$  dyn·cm and an  $M_w$  of 7.9. Bakun (1999) considers  $M$  7.8 to be a mean magnitude for 1906 and uses two methods to estimate moment in the SFBR from it. One method assumes constant moment release along the rupture and calculates its value for the length of the fault in the SFBR. The other uses the average 1906 geodetic slip along the San Andreas (Thatcher *et al.*, 1997) within the SFBR and a fault width of 10 km. The estimated moments from these methods are  $2.82 \times 10^{27}$  dyn·cm and  $2.88 \times 10^{27}$  dyn·cm, respectively, for 1906 within the SFBR, and Bakun (1999, his table 3) averages them for a moment of  $2.85 \times 10^{27}$  dyn·cm.

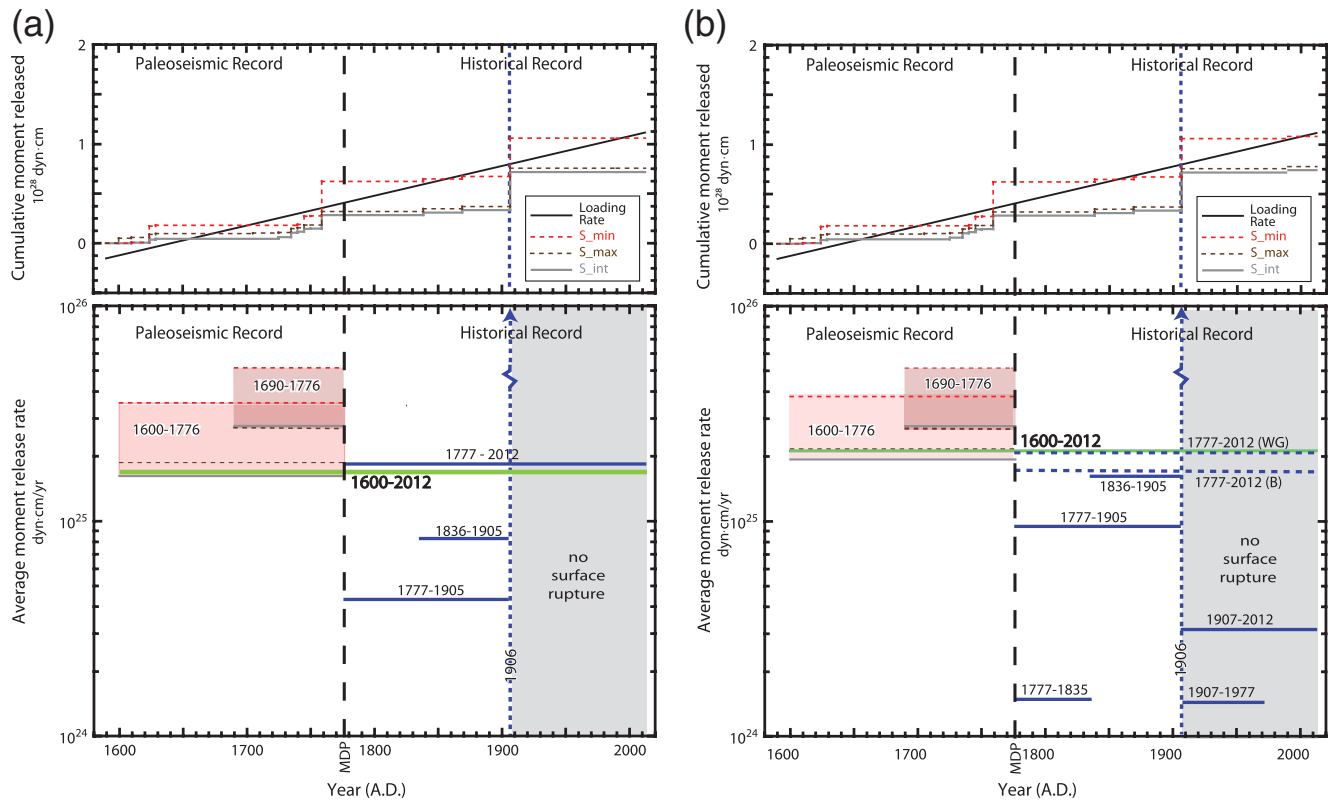


**Figure 5.** Models of seismic moment release ( $\Sigma M_0/\text{yr}$ ) in the SFBR for the interval 1600–2012. (a) Moment release rates for different time intervals from surface-faulting events only. Horizontal lines are  $\Sigma M_0/\text{yr}$  over specified interval. Shaded rectangles are bound rates from the three paleoseismic rupture sequences; the dashed red line is  $S_{\min}$ , dashed black line is  $S_{\max}$ , and solid gray line is  $S_{\text{int}}$ . The large rectangle is 1600–1776; and the small rectangle is the 1690–1776 cluster. The solid green line is the preferred mean  $\Sigma M_0/\text{yr}$  of  $1.75 \times 10^{27}$  dyn·cm from surface-faulting earthquakes. Note the decrease in large-earthquake moment release between the end of the cluster and 1906. The 1777–2012 interval is dominated by the 1906 moment release, which cannot be plotted at the scale of the figure. Since 1906, there have been no large surface-faulting earthquakes on the major SFBR plate boundary faults. The upper part of the figure is a plot of the cumulative moment release from paleoseismic and historical surface-faulting earthquakes. Steps in the cumulative moment release accompany the 1690–1776 cluster and 1906 earthquake. The solid line is the long-term average moment release rate derived from [Argus and Gordon \(2001\)](#). (b)  $\Sigma M_0/\text{yr}$  from combined paleoseismic and historical seismic records. Symbols are the same as for (a). The  $\Sigma M_0/\text{yr}$  for different intervals between 1600–2012 combine moment from surface-faulting earthquakes, moment estimated by [Bakun \(1999\)](#) from historical seismicity, and our estimates of moderate event seismicity during the 1600–1776 paleoseismic and 1777–1835 early historical intervals. Two rates of moment release are shown for 1777–2012. The higher-value dashed line (WG) uses the 1906 moment release in the SFBR based on [WGCEP \(2003\)](#) fault parameters; the lower-value dashed line (B) is based on the [Bakun \(1999\)](#) estimate of the 1906 moment release in the SFBR. The solid green line is the preferred mean for 1600–2012  $\Sigma M_0/\text{yr}$  of  $2.21 \times 10^{27}$  dyn·cm for the combined model of surface-faulting earthquakes and seismicity.

From the slip values of [Song \*et al.\* \(2008\)](#), their electronic supplement), we calculate an average slip of 3.91 m along 246 km of the rupture in the SFBR. Using a fault width of 12 km ([Song \*et al.\*, 2008](#)) produces a seismic moment of  $3.46 \times 10^{27}$  dyn·cm. For the same length of fault, the seismogenic area parameters of [WGCEP \(2003\)](#) yield a mean moment of  $3.82 \times 10^{27}$  dyn·cm. This higher moment reflects a wider fault plane used for the Peninsula (13 km) and Santa Cruz Mountains (15 km) segments. This is the seismic moment preferred in this paper (1906 SFBR, Table 5) because it uses the same fault area parameters as our estimates of magnitude and moment for the paleoearthquakes, and it is the value used in the surface-faulting-only model of moment release (Fig. 5a). Both it and the [Bakun \(1999\)](#) estimates are used to develop alternative moment release rates for the

1777–2012 interval in the combined paleoseismic and historical seismicity model (Fig. 5b).

The sums of the moment ( $\Sigma M_0$ ) and the moment rates per year ( $\Sigma M_0/\text{yr}$ ) for selected time intervals between 1600 and 2012 are listed in Table 6, and the rates are shown graphically in Figure 5. For the paleoseismic events, moment sums and release rates are developed from the three chronologic source models ( $S_{\min}$ ,  $S_{\text{int}}$ ,  $S_{\max}$ ) from 1600 to 1776 and for the 1690–1776 cluster. From 1600 through 1776, the estimated mean paleoseismic  $\Sigma M_0/\text{yr}$  for the range of models is  $1.60 \times 10^{25}$  to  $3.53 \times 10^{25}$  dyn·cm/yr. The higher rate reflects the multisegment ruptures of the minimum source model. The rates for the maximum and intermediate source models are comparable. Our preferred rate for this interval is  $1.60 \times 10^{25}$  dyn·cm/yr, which is derived from the intermediate source model. The long-term moment release rate

estimate (1600–2012) incorporates the paleoseismic moment (1600–1776), the moment for the 1838 and 1868 earthquakes (1777–1905), and the 1906 moment release in the SFBR using the [WGCEP \(2003\)](#) seismogenic source area. The 1989 Loma Prieta earthquake, which did not rupture the surface, is not included in this estimate. Using the  $\Sigma M_0$  for the intervals noted above (Table 6), the preferred long-term (1600–2010)  $\Sigma M_0/\text{yr}$  for the SFBR is  $1.75 \times 10^{25}$  dyn·cm/yr (Fig. 5a), with a range of  $1.60\text{--}2.58 \times 10^{25}$  dyn·cm/yr (derived from the values in Table 6).

In comparing various intervals with the long-term release rate, the preferred rate for 1660–1776 ( $S_{\text{int}}$ ) is slightly below the long-term average. The preferred mean  $\Sigma M_0/\text{yr}$  during the 1690–1776 cluster is  $2.72 \times 10^{25}$  dyn·cm/yr (with a range of  $2.65\text{--}5.14 \times 10^{25}$  dyn·cm/yr), which is well above the long-term rate (Fig. 5a). Between 1777 and the 1906 earthquake, only two large events, in 1838 and 1868, occurred in the SFBR. The mean magnitude estimate of  $M$  6.8 for each ([Bakun, 1999](#)) yields a  $\Sigma M_0/\text{yr}$  of  $2.78 \times 10^{24}$  dyn·cm/yr for this interval. A shorter part of the interval, 1836–1905, has a  $\Sigma M_0/\text{yr}$  of  $8.50 \times 10^{24}$  dyn·cm/yr. Both are well below the long-term rate (Fig. 5a). The 1906 earthquake produced a major spike in moment release. This was followed by a 107-year (and counting) interval of low seismicity during which there have been no surface-faulting earthquakes. The mean  $\Sigma M_0/\text{yr}$  for the 1777–2012 interval is  $1.88 \times 10^{25}$  dyn·cm/yr (Table 6, Fig. 5a). This is not significantly different from the 1600–1776 interval ( $S_{\text{int}}$  and  $S_{\text{max}}$  models) and is essentially the same as the mean long-term rate. This set of calculations suggests the long-term release rate, with regard to geologically estimated magnitudes of surface ruptures of the main plate boundary faults, is relatively constant. The large-earthquake  $\Sigma M_0/\text{yr}$  for the 1777–1905 interval is low, at  $4.56 \times 10^{24}$  dyn·cm/yr. Although there has not been a large surface-faulting earthquake since 1906, the inclusion of the blind 1989  $M$  6.9 Loma Prieta earthquake as a surrogate for a surface-faulting event would give a comparably low rate of  $2.38 \times 10^{24}$  dyn·cm/yr for 1907–2012 (Table 6). Each of these low-rate intervals follows a substantial release of moment in the SFBR. This is also clearly seen in the plot of cumulative moment released in the SFBR (upper part of Fig. 5), in which significant step increases in cumulative moment from the 1690–1776 cluster and from 1906 are followed by intervals of low-cumulative moment release.

*Combined  $\Sigma M_0/\text{yr}$  in Surface-Faulting and Moderate ( $M \leq 5 + M \geq 5.5$ ) Earthquakes.* Figure 3c shows the SFBR paleoearthquake sequence from the intermediate source model, plus the dates and mean magnitudes of smaller earthquakes extending back to 1836 ([Bakun, 1999](#)). As part of his comprehensive analysis of SFBR seismicity prior to and following the 1906 earthquake (1836–1997), [Bakun \(1999\)](#) estimates  $\Sigma M_0$  and calculates  $\Sigma M_0/\text{yr}$  for different intervals of time within the historical record. We use these, along with our paleoseismic estimates, to expand the view of moment release through time in the SFBR. Those relevant to

the present analysis are listed in Table 6 and are incorporated in Figure 5b. The distribution of  $\Sigma M_0/\text{yr}$  from the historical record is quite variable, depending on the interval of time selected. We extrapolate the estimates of [Bakun \(1999\)](#) backward to 1777, with some assumptions about frequency of moderate events during the early historical period, and we speculate on the frequency of these smaller earthquakes during the 1600–1776 paleoseismic interval.

The frequency of moderate events during the 1600–1776 paleoseismic interval, and into the early 1800s, is not known. It has been suggested that the post-1850 to pre-1906 seismicity represents accelerated moment release prior to the 1868 Hayward fault and 1906 earthquakes ([Sykes and Jaume, 1990](#); [Bufe and Varnes, 1993](#); [Bebbington et al., 2010](#)). It is reasonable that moderate seismicity occurred in the interval leading up to the paleoseismic cluster. To account for this, we have used the moment rate from the 1836–1905 interval minus the 1838 and 1868 earthquakes (Table 6) and added it to the paleoseismic record for the 90 years prior to 1690 (which contains the events of similar or larger magnitudes as 1838 and 1868). This increases the total moment and the moment rates for the  $S_{\text{int}}$  and  $S_{\text{max}}$  paleoseismic sequences by about 20%, and for  $S_{\text{min}}$  about 5%, above the surface-faulting-only estimates (Table 6, Fig. 5b).

From 1777 to 1835, there are no known large events, but smaller earthquakes did occur, with at least seven reported between October 1800 and September 1829 ([Townley and Allen, 1939](#)). For this 58-year interval immediately following the cluster, we assume the moment rate is low and adopt the rate calculated by [Bakun \(1999\)](#) for SFBR moment release during a 71-year period following 1906 ([Bakun, 1999](#)) (Table 6).

[Bakun \(1999\)](#) estimates a mean  $\Sigma M_0/\text{yr}$  of  $2.33 \times 10^{25}$  dyn·cm/yr in the SFBR from 1836 to 1998. Using 1906 SFBR moment from the [WGCEP \(2003\)](#) mean fault area (Table 5) results in a rate of  $3.3 \times 10^{25}$  dyn·cm/yr for the same interval. Extending both of these to 1777 with the lower release rate estimated above for that interval (Table 6), and to 2012, yields  $\Sigma M_0/\text{yr}$  of  $1.80 \times 10^{25}$  dyn·cm/yr and  $2.21 \times 10^{25}$  dyn·cm/yr, respectively (Fig. 5b).

For 1600 to 2012, the addition of combined paleoseismic and seismologic moment estimates from the three source models gives long-term  $\Sigma M_0/\text{yr}$  of  $2.21 \times 10^{25}$  dyn·cm/yr,  $2.25 \times 10^{25}$  dyn·cm/yr, and  $2.81 \times 10^{25}$  dyn·cm/yr, respectively, for the intermediate (preferred), maximum, and minimum source models. The estimated long-term combined release rate is similar to, though slightly higher (21%) than, the surface-faulting-only rate, as would be expected with the addition of moment from smaller earthquakes. Comparison of Figure 5a and 5b shows a qualitatively similar pattern of moment release. In Figure 5b, following the paleoseismic cluster, the moment release rate from 1777 through 1905 remains below the long-term average, even though the addition of post-1836 moderate events add significant moment (equivalent to one  $M_w$  7.2 earthquake) during this interval.

Table 7

Comparison of the Sum of the Moment ( $\Sigma M_0$ ) for Paleoseismic Rupture Source Sequences Versus 1906 Moment Release in the SFBR

Paleoseismic Rupture Source Sequence*	$\Sigma M_0$ Mean ( $10^E$ dyn-cm) <sup>†</sup>	Paleoseismic/1906 ( $2.85 \times 10^{27}$ ) (%) <sup>‡</sup>	Paleoseismic/1906 ( $3.82 \times 10^{27}$ ) (%) <sup>§</sup>
$S_{\min}$ (1600–1776)	6.21 <sup>27</sup>	219	163
$S_{\min}$ (1690–1776)	4.42 <sup>27</sup>	155	116
$S_{\max}$ (1600–1776)	3.26 <sup>27</sup>	114	85
$S_{\max}$ (1690–1776)	2.28 <sup>27</sup>	80	52
$S_{\text{int}}$ (1600–1776)	2.81 <sup>27</sup>	98	74
$S_{\text{int}}$ (1690–1776)	2.34 <sup>27</sup>	82	61

\*Listed in Table 3.

<sup>†</sup>Listed in Table 5.

<sup>‡</sup>Preferred moment (dyn-cm) of Bakun (1999, his table 3) for 1906 in SFBR.

<sup>§</sup>1906 moment (dyn-cm) in SFBR from WGCEP (2003) fault parameters.

$\Sigma M_0$  of the Paleoseismic Sequence and Comparison to 1906. An important comparison is the  $\Sigma M_0$  for the paleoseismic interval, particularly the cluster, and the moment released in the SFBR in 1906. Table 6 lists a range of estimates for each, and these are shown graphically as cumulative moment from surface-rupturing earthquakes in the upper part of Figure 5. For the paleoseismic interval, the  $\Sigma M_0$  ranges from  $2.81 \times 10^{27}$  to  $6.21 \times 10^{27}$  dyn-cm (Table 6). As noted previously, for 1600–1776 our preference is the  $S_{\text{int}}$  model, with  $\Sigma M_0$  of  $2.81 \times 10^{27}$  dyn-cm. For the more temporally limited cluster (1690–1776), the  $\Sigma M_0$  ranges from  $2.28 \times 10^{27}$  to  $4.42 \times 10^{27}$  dyn-cm, with our preferred  $S_{\text{int}}$   $\Sigma M_0$  of  $2.34 \times 10^{27}$  (Table 6). The values for  $S_{\max}$  are quite comparable. The  $\Sigma M_0$  for 1600–1776 (all models) is a minimum if during this period additional large earthquakes occurred on the Greenville fault or northern extension of the Concord–Green Valley fault, or if the 1750 San Andreas rupture that we have restricted to the San Juan Bautista segment (Appendix A) actually ruptured through the Santa Cruz Mountains.

The estimates of moment released in the SFBR in 1906 range from  $2.82 \times 10^{27}$  to  $3.82 \times 10^{27}$  dyn-cm. Table 7 lists the percentage of paleoseismic  $\Sigma M_0$  relative to 1906 SFBR moment for different paleoseismic source models and 1906 moment values. In this comparison, we use the Bakun (1999) estimate of 1906 SFBR moment of  $2.85 \times 10^{27}$  for the lower value and the moment based on WGCEP (2003) fault parameters and presented here (Table 5) at the upper end. The  $\Sigma M_0$  for the longer 1600–1776 paleoseismic interval varies from 74% to 219% of 1906. For the 1690–1776 cluster, the range is 52%–116%. The percentages for the  $S_{\min}$  model seem very high. The  $\Sigma M_0$  from the paleoseismic sequence is slightly lower than (though, given the uncertainties, comparable to) 1906 for the preferred  $S_{\text{int}}$  and the similar  $S_{\max}$  source sequences. The plot of cumulative moment (upper panel of Fig. 5) clearly shows the similarity in the increase in moment release associated with both the 1690–1776 cluster and the 1906 surface rupture, and the lower moment rate that followed each.

## Earthquake Cycles and Stress Shadows

One of the basic characteristics ascribed to the earthquake cycle is the decrease in the rate of seismic activity on a regional scale following a great earthquake. The SFBR has figured prominently in the development of this concept with the observation that the rate of moderate ( $M \geq 5.5$ ) earthquakes was significantly higher in the decades prior to the 1906 earthquake than in the period following it (Tocher, 1959; Ellsworth *et al.*, 1981; Simpson and Reasenberg, 1994; Jaume and Sykes, 1996). Bakun (1999) concludes that in the 70 years before the 1906 earthquake (1836–1906), there had been  $\geq 55$  earthquakes of  $M \geq 4.6$ , of which 9 were  $M \geq 6.2$ ; in contrast, during the 90 years from 1906 through 1997, there were 17 events of  $M \geq 5.3$  with 3 earthquakes of  $M \geq 6.2$ . In addition, he calculates the  $\Sigma M_0/\text{yr}$  in the 56 years before 1906 is approximately 10 times the rate for the 70 years after. This change in seismicity rate in the SFBR has been termed as a stress shadow (Simpson and Reasenberg, 1994).

The various phases suggested for the earthquake cycle, such as an increase of seismicity prior to a great earthquake or decrease following one, are based on a generally short record of earthquake occurrence. The length of the record of large earthquakes in the SFBR discussed here, approximately 400 years, is more than twice the length of the historical record. Figure 3 shows that between 1600 and our historical cutoff of 1776 (and even if cutoff uncertainty is extended to 1800), there were anywhere from 7 to 11 surface-faulting earthquakes in a maximum interval of 176 years (one per 16–25 years) and possibly from 4 to 7 events in an interval of 86 years (1690–1776) or less (one per 12–21 years). Not only does the frequency of small earthquakes change over time, it appears from this longer record that the frequency of  $M \geq 6.5$  events can also vary considerably. Using these paleoseismic interpretations, we look at the SFBR from the perspective of a more complete and possibly a full earthquake cycle—one that includes primary seismic moment release in two distinct ways. These are as a single-fault great earthquake (such as 1906) and as a temporal cluster of large earthquakes that we have interpreted from the paleoseismic record.

There is little disagreement that the regional rate of seismicity dropped abruptly after 1906, but there is a considerable difference of opinion about the physical controls and duration of this quiescence in the SFBR. Harris and Simpson (1998) suggest that static Coulomb stress changes affecting the stress on regional faults parallel to the San Andreas could explain the post-1906 quiescence. Kenner and Segall (1999) analyze the 1906 stress shadow and its duration using four geometric and rheological models. They suggest the stress shadow can be a time-dependent process reflecting structure and rheology of the lower crust and mantle. Without giving specific time estimates, Kenner and Segall (1999) conclude that the duration of the shadow will largely depend on the connectivity of parallel fault structures in the lower crust.

Parsons (2002) analyzes the stress shadow through a finite element model that uses a range of stressing distributions for SFBR faults and intervening crust, as well as postseismic effects such as deep afterslip and viscoelastic relaxation in the upper mantle. Parsons (2002) notes the duration of the stress shadow decreases on each SFBR fault with increasing distance from the 1906 rupture. For the finite element model the duration of the stress shadow is 11 to 56 years if viscoelastic effects are neglected, and 17 to 74 years if they are included, depending on the fault. This contrasts with a dislocation loading model for which the duration of the shadow on individual faults is between 7 and 54 years.

In the analyses cited, the primary cause of the stress shadow is the stress change from a combination of short-term static and longer-term viscoelastic stress interactions, and the modeling suggests that the shadow effect should have ended. Yet in the SFBR, seismic quiescence is ongoing, which led Reasenber *et al.* (2003) to propose an empirical model to account for continuing stress shadow effects in the calculation of SFBR probabilities by WGCEP (2003). The chronology of SFBR surface-faulting earthquakes provides a basis to suggest that factors other than stress change may play a role in producing or increasing the duration of a period of regional seismic quiescence.

Pollitz and Schwartz (2008) present a model of stress evolution in the SFBR that is based in part on an earlier version of the paleoearthquake chronology described here. They suggest that through static and viscoelastic interactions, a rupture sequence beginning in 1656 (an arbitrary date for the analysis) produced stress shadows around individual faults that by 1776 cumulatively resulted in a regional stress decrease comparable to the regional stress decrease following 1906. Comparisons of the modeled stress in the SFBR in 1770 and 1910 are shown in Figure 6. Figure 3 illustrates the relatively infrequent occurrence of large earthquakes in the SFBR between 1776 and 1906. Subsequent to the paleoseismic cluster, the average moment release per year, even including the post-1836 moderate events (Fig. 5b), was below the long-term average until 1906. Qualitatively the post-1776 decrease in moment release per year is not substantially different from the decrease following 1906. However, it resulted from multiple events on subparallel faults over a period of time rather than from a single great rupture.

Although stress changes and fault interactions clearly play a major role, we suggest that part of the stress shadow process, and a possible control on its duration, is the regional depletion of accumulated strain in the event or events that culminate a cycle. It simply requires time, possibly longer than the effect of stress changes alone, to re-accumulate this. As noted, the cumulative moment released by the seventeenth to eighteenth century paleoearthquakes (with the major percentage between 1690 and 1776) and the moment of 1906 in the SFBR are comparable within the uncertainties presented. The 1906 earthquake was the result of slip on one fault, with an average of 4.1 m (Song *et al.*, 2008) along the full length of the rupture and 3.91 m (our calculation) in the SFBR. With a

regional stressing rate of 40 mm/yr (a reasonable midpoint for the various estimates), approximately 5.2 m of slip would have accumulated in the SFBR between 1776 and 1906, given no other release outlet. Some percentage of this slip was released in the 1838 and 1868 earthquakes, additional slip occurred during the moderate historical events, and some was released through creep. However, clearly by 1906, the SFBR crustal volume had reloaded sufficiently to initiate failure of the system, and perhaps 4 m is the critical level required. If this is the case, then the time necessary to reach this level may extend beyond the temporal influence of both coseismic and postseismic stress changes.

## Conclusions

The paleoseismic record of surface-faulting earthquakes provides a unique opportunity to extend our understanding of the process of plate boundary stress accumulation and release—the earthquake cycle—well beyond the historical seismic record. Paleoseismic studies of the major faults in the SFBR have given us a nearly complete inventory of large ruptures since 1600. From the analysis developed here, we estimate these surface ruptures are associated with earthquakes ranging in magnitude (mean) from about  $M \geq 6.6$  to about  $M 7.8$ . The paleoearthquake chronology from 1600 to 1776 (the beginning of the historical record of large earthquakes with the founding of the Mission Dolores and Presidio in San Francisco) provides evidence for rupture of the San Andreas fault (North Coast plus Offshore, Santa Cruz Mountains, and San Juan Bautista segments), Hayward fault (twice on the southern Hayward with the penultimate likely including the northern Hayward), Rodgers Creek fault, San Gregorio fault, northern Calaveras fault, and Concord–Green Valley fault. The evidence for the extent and location of rupture on the Peninsula segment of the San Andreas fault during this interval is equivocal, and there are no paleoearthquake data for the Greenville fault or northern extension of the Concord–Green Valley fault.

Perhaps the most intriguing, and a quite robust, observation is that a subset of these paleoearthquakes appears to have occurred as a cluster of events along the major SFBR plate boundary faults between the mid to late-seventeenth and late-eighteenth centuries. It includes the North Coast San Andreas, southern and northern Hayward, Rodgers Creek, northern Calaveras, San Gregorio, and San Juan Bautista ruptures. Two-sigma OxCal-modeled radiocarbon age ranges allow a combined southern and northern Hayward fault rupture to have occurred as early as 1658, although it was likely in the eighteenth century, and they constrain the remaining ruptures to post-1690. Historical constraints cap the occurrence of these paleoearthquakes at 1776.

Estimates of the preferred  $\Sigma M_0/\text{yr}$  for the 1660–2012 interval range from  $1.75 \times 10^{25}$  dyn·cm/yr from modeling only surface-faulting earthquakes to  $2.21 \times 10^{25}$  dyn·cm/yr from a combination of surface ruptures and seismicity. A major result of our analysis is that the SFBR earthquake

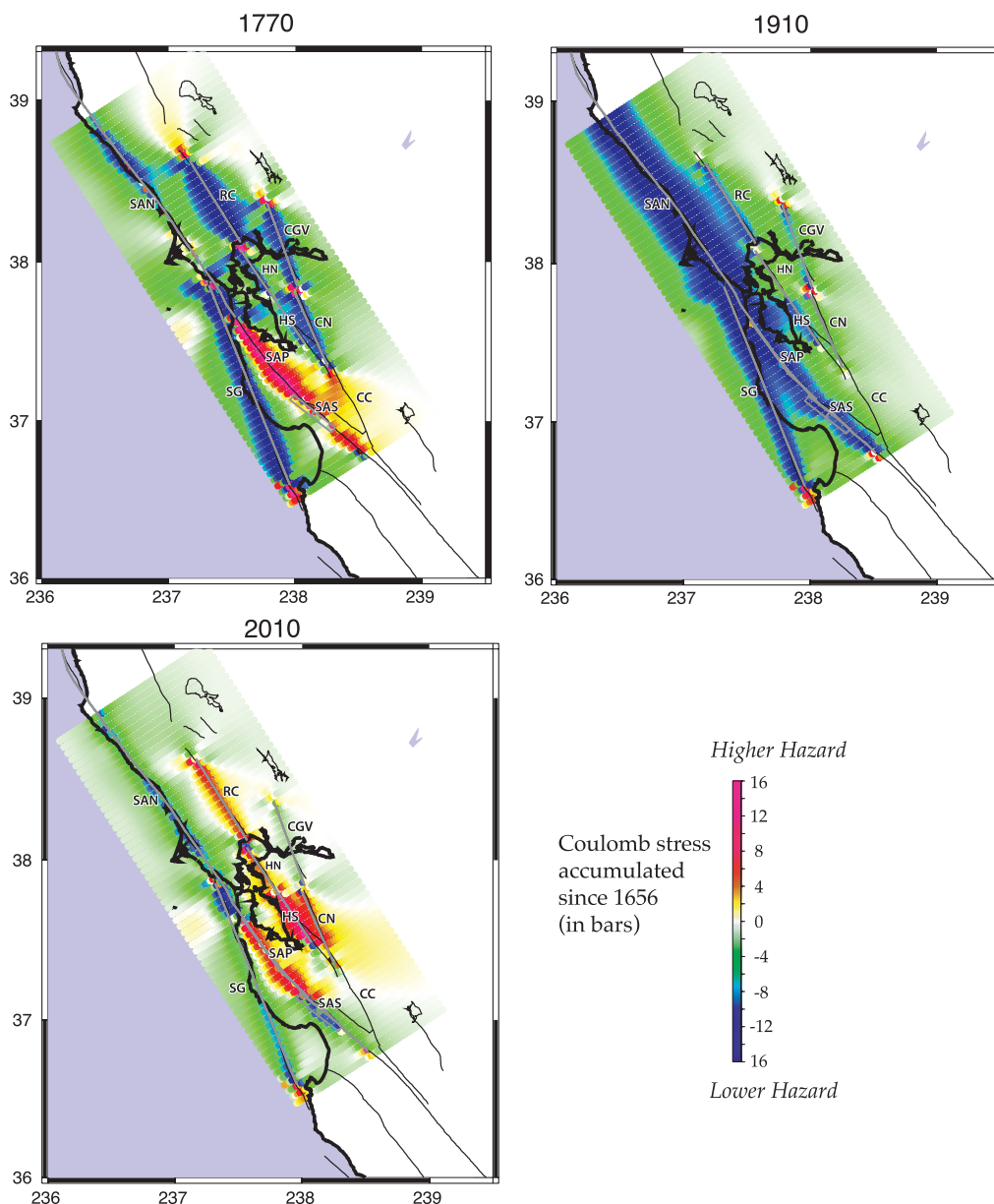


**Figure 6.** Snapshots of modeled cumulative stress changes in the SFBR. Three time slices from a stress evolution model extending from 1660 to 2040 are shown (modified from Pollitz and Schwartz, 2008). The warmer colors indicate increased Coulomb stress, and the cooler colors define decreased stress. The time slice for 1770 shows the regional decrease in stress following a sequence of large earthquakes similar to that described here. The time slice for 1910 shows the modeled stress in the SFBR following the 1906 earthquake. The time slice at 2010 reflects the general increase in stress across the SFBR at essentially the present time.

cycle—the release of seismic moment in the form of large and damaging earthquakes—varies considerably over time. Although the regional plate tectonic stressing rate, within uncertainties, remains constant, its release in SFBR crust can occur in one great event like 1906, or it can be distributed across the region as rupture of the primary plate boundary faults during a relatively short, decadal interval. This appears to have been the case during the most recent full cycle, and variations likely occur. The estimated mean  $\Sigma M_0$  from the beginning of our paleoearthquake chronology in 1600 to the beginning of the historical record of large earthquakes in

1776 ranges from  $2.81 \times 10^{27}$  to  $6.21 \times 10^{27}$  dyn·cm. The mean  $\Sigma M_0$  estimated for the 1690–1776 cluster is  $2.28 \times 10^{27}$  to  $4.42 \times 10^{27}$  dyn·cm. The cluster was followed by a 128-year period of quiescence for large surface-rupturing earthquakes on the primary plate boundary faults in the SFBR, with only the 1868 Hayward fault rupture occurring on one with certainty. The seismic moment of the 1906 earthquake within the SFBR is variously estimated at 2.82 to  $3.82 \times 10^{27}$  dyn·cm. To date, the 1906 event has been followed by a 107-year interval during which no large plate boundary strike-slip surface ruptures have occurred. The only

large event during this period was the 1989  $M$  6.9 Loma Prieta earthquake, which occurred on a blind reverse-oblique slip rupture adjacent to the San Andreas fault. The similarity in the limited occurrence of surface-rupturing plate boundary fault earthquakes following a large regional moment release in two different ways suggests the re-accumulation of regional stress to a critical failure level for the system is a long process that eventually overrides the waning influence of both coseismic and postseismic stress changes.

To date, the accumulated system-wide slip deficit in the SFBR since 1906 is approximately 4 m, with a small percentage already released through creep and the Loma Prieta earthquake. By 2036, it will be 5 m. The [WGCEP \(2003\)](#) calculated a 62% probability of one or more  $M \geq 6.7$  earthquakes in the SFBR between 2002 and 2031. The [WGCEP \(2008\)](#) revised this to 63% between 2007 and 2036. These probabilities are distributed on faults across the SFBR, with a very small likelihood of a 1906 repeat during these time intervals. There is no guarantee what path the occurrence of future large earthquakes in the SFBR will take, but given the earthquake history since 1600, there is a strong likelihood that it will be more similar to the paleoseismic cluster—the plate boundary faults have to slip—than to 1906. This is conceptually consistent with the Working Group probabilities.

### Data and Resources

All data and resources used in the development of the observations and interpretations presented here are openly available in the cited references, with the exceptions of [Kelson and Baldwin \(2000a,b,c\)](#), [Kelson and Randolph \(2000\)](#), and [Simpson and Knudsen \(2000\)](#), which are unpublished contract reports written for the U.S. Geological Survey.

A primary source for the SFBR fault characterization developed in this paper is USGS Open-File Report 03-214, *Earthquake Probabilities in the SFBR: 2002–2031*. The full report can be downloaded at [http://pubs.usgs.gov/of/2003/of03-214/OFR-03-214\\_FullText.pdf](http://pubs.usgs.gov/of/2003/of03-214/OFR-03-214_FullText.pdf) (last accessed August 2013).

Chapter 3 of the USGS report, “Characterization of the SFBR Earthquake Sources,” provides details of the SFBR fault segmentation model used in this paper and includes 10 figures with maps detailing the segments and their boundaries. This can be downloaded directly at [http://pubs.usgs.gov/of/2003/of03-214/WG02\\_OFR-03-214\\_Chapter3.pdf](http://pubs.usgs.gov/of/2003/of03-214/WG02_OFR-03-214_Chapter3.pdf) (last accessed August 2013).

Chapter 4 of the USGS report, “The SFBR Earthquake Source Model: Magnitudes and Long-Term Rates,” can be downloaded at [http://pubs.usgs.gov/of/2003/of03-214/WG02\\_OFR-03-214\\_Chapter4.pdf](http://pubs.usgs.gov/of/2003/of03-214/WG02_OFR-03-214_Chapter4.pdf) (last accessed August 2013).

The Calib 7.0 radiocarbon calibration program can be accessed at <http://calib.qub.ac.uk/calib/calib.html> (last accessed October 2013).

### Acknowledgments

We appreciate the thorough reviews of Timothy Dawson, Fred Pollitz, Jeff Ritz, Yann Klinger, and an anonymous reviewer. Much of the paleoseismic data discussed here are the direct outgrowth of investigations initiated by the Bay Area Paleoequake Experiment (BAPEX), part of a Cooperative Research and Development Agreement (CRADA) between the U.S. Geological Survey (USGS) and the Pacific Gas and Electric Company, to increase understanding of earthquake sources in the San Francisco Bay Region (SFBR). In regard to this, we thank Lloyd Cluff for his foresight and support of this effort. A special thank you goes to the paleoseismologists and earthquake geologists who have worked, and are still working, to extend the earthquake history of the SFBR back in time.

### References

- Argus, D. F., and R. G. Gordon (2001). Present tectonic motion across the Coast Ranges and San Andreas fault system in central California, *Geol. Soc. Am. Bull.* **113**, 1580–1592.
- Bakun, W. H. (1999). Seismic activity of the San Francisco Bay region, *Bull. Seismol. Soc. Am.* **89**, 764–784.
- Bakun, W. H., and C. M. Wentworth (1997). Estimating earthquake location and magnitude from seismic intensity data, *Bull. Seismol. Soc. Am.* **87**, 1502–1521.
- Baldwin, J. N., K. I. Kelson, and C. E. Randolph (1998). Timing of the most-recent surface faulting event on the northern Calaveras fault, near Sunol, California [abs.], *Eos Trans. AGU* **79**, no. 4 (Fall meeting).
- Baldwin, J. N., K. L. Knudsen, A. Lee, C. S. Prentice, and R. Gross (2000). Preliminary estimate of coseismic displacement of the penultimate earthquake on the northern San Andreas fault, Pt. Arena, California, in *Tectonic Problems of the San Andreas Fault System*, G. Bokelman and R. Kovachs (Editors), Stanford University Publications, Stanford, California, Geological Sciences, Vol. XXI, 355–368.
- Baldwin, J. N., R. Turner, and J. J. Lienkaemper (2008). Earthquake record of the Green Valley fault, Lopes Ranch, Solano County, California, *U.S. Geological Survey, National Earthquake Hazards Reduction Program*, Final Technical Report Award Number 06HQGR0144, 39 pp.
- Bebbington, M. S., D. S. Harte, and S. C. Jaume (2010). Repeated intermittent earthquake cycle in the San Francisco Bay region, *Pure Appl. Geophys.* **167**, 801–818, doi: [10.1007/s00024-010-0064-6](https://doi.org/10.1007/s00024-010-0064-6).
- Bowman, D. D., and G. C. P. King (2001). Accelerating seismicity and stress accumulation before large earthquakes, *Geophys. Res. Lett.* **28**, 4039–4042.
- Bronk Ramsey, C. (2001). Development of the radiocarbon calibration program OxCal, *Radiocarbon* **43**, no. 2a, 355–363.
- Bronk Ramsey, C. (2007). *OxCal Program, v. 4.0*, Radiocarbon Accelerator Unit, University of Oxford, United Kingdom.
- Budding, K. E., D. P. Schwartz, and D. H. Oppenheimer (1991). Slip rate, earthquake recurrence, and seismogenic potential of the Rodgers Creek fault zone, northern California: Initial results, *Geophys. Res. Lett.* **18**, 447–450.
- Bufe, C. G., and D. J. Varnes (1993). Predictive modeling of the seismic cycle in the greater San Francisco Bay region, *J. Geophys. Res.* **98**, 9871–9883.
- Bürgmann, R., D. Schmidt, R. M. Nadeau, M. d’Alessio, E. Fielding, D. Manaker, T. V. McEvilly, and M. H. Murray (2000). Earthquake potential along the northern Hayward fault, *Science* **289**, 1178–1182.
- Cotton, W. R., N. T. Hall, and E. A. Hay (1982). Holocene behavior of the San Andreas fault at Dogtown, Point Reyes National Seashore, California, *National Earthquake Hazards Reduction Program Final Technical Report*, Contract 14-08-0001-19841, 33 pp.
- d’Alessio, M., I. A. Johanson, R. Bürgmann, D. A. Schmidt, and M. H. Murray (2005). Slicing up the San Francisco Bay area: Block kinematics and fault slip rates from GPS-derived surface velocities, *J. Geophys. Res.* **110**, no. B06403, doi: [10.1029/2004JB003496](https://doi.org/10.1029/2004JB003496).

- DeMets, C., R. G. Gordon, D. F. Argus, and S. Stein (1994). Effect of recent revisions to the geomagnetic reversal time scale on estimates of current plate motions, *Geophys. Res. Lett.* **21**, 2191–2194.
- Ellsworth, W. L., A. G. Lindh, W. H. Prescott, and D. G. Herd (1981). The 1906 San Francisco earthquake and the seismic cycle, in *Earthquake Prediction, An International Review*, D. W. Simpson and P. G. Richards (Editors), Maurice Ewing Series 4, American Geophysical Union Monograph, Washington, D.C., 126–140.
- Fumal, T. E. (2012). Timing of large earthquakes during the past 500 years along the Santa Cruz mountains segment of the San Andreas fault at Mill Canyon, near Watsonville, California, *Bull. Seismol. Soc. Am.* **102**, 1099–1119.
- Fumal, T. E., T. E. Dawson, R. Flowers, J. C. Hamilton, G. F. Heingartner, J. Kessler, and L. Samrad (2004). Photomosaics and logs of trenches on the San Andreas fault at Mill Canyon near Watsonville, California, *U.S. Geol. Surv. Open-File Rept.* 03-469, 1 sheet.
- Fumal, T. E., G. F. Heingartner, T. E. Dawson, R. Flowers, J. C. Hamilton, J. Kessler, L. M. Reidy, L. Samrad, G. G. Seitz, and J. Southon (2003). A 100-year average recurrence interval for the San Andreas fault, southern San Francisco Bay area, California (abstract S12B-0388), *Eos Trans. AGU* **84**, no. 46 (Fall Meet. Suppl.), F1003, S12B-0388.
- Fumal, T. E., G. F. Heingartner, L. Samrad, T. E. Dawson, J. C. Hamilton, and J. N. Baldwin (2004). Photomosaics and Logs of Trenches on the San Andreas Fault at Arano Flat near Watsonville, California, *U.S. Geol. Surv. Open-File Rept.* 03-450, 3 sheets.
- Gilbert, G. K. (1884). A theory of the earthquakes of the Great Basin, with a practical application, *Am. J. Sci. Ser. 3* **27**, no. 157, 49–54.
- Gillespie, R. (1984). *Radiocarbon User's Handbook*, Oxford Univ. Comm. for Archaeol., Oxbow Books, Oxford, England, 154 pp.
- Goldfinger, C., K. Grijalva, R. Bürgmann, A. E. Morey, J. E. Johnson, C. H. Nelson, J. Gutiérrez-Pastor, A. Ericsson, E. Karabanov, J. D. Chaytor, J. Patton, and E. Gràcia (2008). Late Holocene rupture of the northern San Andreas fault and possible stress linkage to the Cascadia subduction zone, *Bull. Seismol. Soc. Am.* **98**, 861–889.
- Goldfinger, C., A. E. Morey, C. H. Nelson, J. Gutiérrez-Pastor, J. E. Johnson, E. Karabanov, J. Chaytor, and A. Eriksson (2007). Rupture lengths and temporal history of significant earthquakes on the Offshore and North Coast segments of the northern San Andreas fault based on turbidite stratigraphy, *Earth Planet. Sci. Lett.* **254**, 9–27.
- Haessler, P. J., D. P. Schwartz, T. E. Dawson, H. D. Stenner, J. J. Lienkaemper, B. Sherrod, F. R. Cinti, P. Montone, P. A. Craw, A. J. Crone, and S. F. Personius (2004). Surface rupture and slip distribution of the Denali and Totschunda faults in the 3 November 2002 M 7.9 earthquake, Alaska, *Bull. Seismol. Soc. Am.* **94**, no. 6, S23–S52.
- Hall, N. T. (1981). The San Andreas fault in Marin County, California: Stops 4, 5, 6, and 7, in *The Franciscan Complex and the San Andreas Fault from Golden Gate to Point Reyes*, in *Pacific Section Book 51*, J. R. Kleist (Editor), American Association of Petroleum Geologists, Tulsa, Oklahoma, 17–28.
- Hall, N. T., and T. M. Niemi (2008). The 1906 earthquake fault rupture and paleoseismic investigation of the northern San Andreas fault at the Dogtown site, Marin County, California, *Bull. Seismol. Soc. Am.* **98**, 2191–2208.
- Hall, N. T., R. H. Wright, and K. B. Clahan (1999). Paleoseismic studies of the San Francisco Peninsula segment of the San Andreas fault zone near Woodside, California, *J. Geophys. Res.* **104**, 23,215–23,236.
- Hanks, T. C., and W. H. Bakun (2002). A bilinear source-scaling model for M log A observations of continental earthquakes, *Bull. Seismol. Soc. Am.* **92**, 1841–1846.
- Hanks, T. C., and W. H. Bakun (2008). M-log A observations for recent large earthquakes, *Bull. Seismol. Soc. Am.* **98**, 490–494.
- Hanks, T. C., and H. Kanamori (1979). A moment magnitude scale, *J. Geophys. Res.* **84**, 2348–2350.
- Harris, R. A., and R. W. Simpson (1998). Suppression of large earthquake by stress shadows: A comparison of Coulomb and rate-and-state failure, *J. Geophys. Res.* **103**, 24,439–24,451.
- Hayward Fault Paleoseismicity Group (1999). Timing of paleoseismicity on the northern Hayward fault—Preliminary evidence in El Cerrito, California, *U.S. Geol. Surv. Open-File Rept.* 99-318, 33 pp.
- Hecker, S., T. E. Dawson, and D. P. Schwartz (2010). Normal-faulting displacement and stress drop variability: A geological perspective, *Bull. Seismol. Soc. Am.* **100**, 3130–3147.
- Hecker, S., D. Pantosti, D. P. Schwartz, J. C. Hamilton, L. M. Reidy, and T. J. Powers (2005). The most recent large earthquake on the Rodgers Creek fault, San Francisco Bay area, *Bull. Seismol. Soc. Am.* **95**, 844–860.
- Hemphill-Haley, M. A., and R. J. Weldon (1999). Estimating prehistoric earthquake magnitude from point measurements of surface rupture, *Bull. Seismol. Soc. Am.* **89**, 1264–1279.
- Jacoby, G. C. (1995). Absolute dating of prehistoric earthquakes by tree-ring analysis in California, *U.S. Geol. Surv. Open-File Rept.* 95-210, 455–458.
- Jaume, S. C., and L. R. Sykes (1996). Evolution of moderate seismicity in the San Francisco Bay region, 1850 to 1993: Seismicity changes related to the occurrence of large and great earthquakes, *J. Geophys. Res.* **101**, 765–789.
- Johanson, I. A., and R. Burgmann (2005). Creep and quakes on the northern transition zone of the San Andreas fault from GPS and InSAR data, *Geophys. Res. Lett.* **32**, L14306, doi: [10.1029/2005GL023150](https://doi.org/10.1029/2005GL023150).
- Kelson, K. I. (2001). Geologic characterization of the Calaveras fault as a potential seismic source, San Francisco Bay area, *Calif. Div. Mines Geol. Spec. Publ.* **212**, 179–192.
- Kelson, K. I., and J. N. Baldwin (2000a). Paleoseismic feasibility study of the northern Calaveras fault at Norris Canyon Road, San Ramon, California, *Final Technical Report submitted to the U.S. Geological Survey Bay Area Paleoseismological Experiment (BAPEX)*, Contract Number 98WRCN1012, CLIN0012, 11 pp.
- Kelson, K. I., and J. N. Baldwin (2000b). Paleoseismic feasibility study of the northern Calaveras fault at Forest Home Farm, San Ramon, California, *Final Technical Report submitted to the U.S. Geological Survey Bay Area Paleoseismological Experiment (BAPEX)*, Contract Number 98WRCN1012, CLIN0013, 16 pp.
- Kelson, K. I., and J. N. Baldwin (2000c). Paleoseismic feasibility study of the northern Calaveras fault at Martin Canyon, Dublin, California, *Final Technical Report submitted to the U.S. Geological Survey Bay Area Paleoseismological Experiment (BAPEX)*, Contract Number 98WRCN1012, CLIN0011, 15 pp.
- Kelson, K. I., and C. E. Randolph (2000). Paleoseismic study of the northern Calaveras fault at 4120 Foothill Road, Pleasanton, California, *Final Technical Report submitted to the U.S. Geological Survey Bay Area Paleoseismological Experiment (BAPEX)*, Contract Number 98WRCN1012, 21 pp.
- Kelson, K. I., and S. T. Sundermann (2007). Digital compilation of northern Calaveras fault data for the Northern California Quaternary Fault Map Database, *Final Technical Report submitted to the U.S. Geological Survey NEHRP*, Award No. 05HQGR0023; <http://earthquake.usgs.gov/research/external/reports/05HQGR0023.pdf> (last accessed August 2013).
- Kelson, K. I., J. S. Hoefft, and M. Buga (2008). Assessment of possible surface rupture on the northern Calaveras fault, eastern San Francisco Bay area, *Final Technical Report, U.S. Geological Survey National Earthquake Hazards Reduction Program*, Award Number 07HQGR0082, 37 pp, <http://earthquake.usgs.gov/research/external/reports/07HQGR0082.pdf> (last accessed August 2013).
- Kelson, K. I., G. D. Simpson, W. R. Lettis, and C. Haraden (1996). Holocene slip rate and earthquake recurrence of the northern Calaveras fault at Leyden Creek, northern California, *J. Geophys. Res.* **101**, 5961–5975.
- Kelson, K. I., R. Streig, R. D. Koehler, and K.-H. Kang (2006). Timing of late Holocene paleoseismicity on the northern San Andreas fault at the Fort Ross Orchard site, Sonoma County, California, *Bull. Seismol. Soc. Am.* **95**, 1012–1028.

- Kenner, S., and P. Segall (1999). Time-dependence of the stress shadowing effect and its relation to structure of the lower crust, *Geology* **27**, 119–122.
- Knudsen, K. L., C. E. Garrison, J. N. Baldwin, G. A. Carver, and W. R. Lettis (1997). Evidence for earthquake-induced, rapid subsidence preserved in estuarine sediment along the North Coast segment of the San Andreas fault (abs.), *GSA Abstr. Programs*, **29**, no. 6, 206.
- Knudsen, K. L., R. C. Witter, C. E. Garrison-Laney, J. N. Baldwin, and G. A. Carver (2002). Past earthquake-induced rapid subsidence along the northern San Andreas fault: A paleoseismological method for investigating strike-slip faults, *Bull. Seismol. Soc. Am.* **92**, 2612–2636.
- Koehler, R. D., R. C. Witter, G. D. Simpson, E. Hemphill-Haley, and W. R. Lettis (2005). Paleoseismic investigation of the northern San Gregorio fault, Half Moon Bay, California, *Final Technical Report, U.S. Geological Survey National Earthquake Hazards Reduction Program*, Award No. 04HQGR0045, 70 pp, <http://earthquake.usgs.gov/research/external/reports/04HQGR0045.pdf> (last accessed August 2013).
- Lawson, A. C. (1908). *The California Earthquake of April 18, 1906, Report of the State Earthquake Investigation Commission*, Vol. 1, Carnegie Inst., Washington, 451 pp.
- Lienkaemper, J. J., and C. Bronk Ramsey (2009). Oxcal: Versatile tool for developing paleoearthquake chronologies—A primer, *Seismol. Res. Lett.* **80**, 431–434.
- Lienkaemper, J. J., and P. L. Williams (2007). A record of large earthquakes on the southern Hayward fault for the past 1800 years, *Bull. Seismol. Soc. Am.* **97**, 1803–1819.
- Lienkaemper, J. J., J. N. Baldwin, R. R. Sickler, R. Turner, and J. Brown (2013). A record of large earthquakes during the past two millennia on the southern Green Valley fault, California, *Bull. Seismol. Soc. Am.* **103**, 2386–2403, doi: [10.1785/0120120198](https://doi.org/10.1785/0120120198).
- Lienkaemper, J. J., T. E. Dawson, S. F. Personius, G. G. Seitz, L. M. Reidy, and D. P. Schwartz (2002). A record of large earthquakes on the southern Hayward fault for the past 500 years, *Bull. Seismol. Soc. Am.* **92**, 2637–2658.
- Lienkaemper, J. J., F. S. McFarland, R. W. Simpson, R. G. Bilham, D. A. Ponce1, J. J. Boatwright, and S. J. Caskey (2012). Long-term creep rates on the Hayward fault: Evidence for controls on the size and frequency of large earthquakes, *Bull. Seismol. Soc. Am.* **102**, 31–41.
- Lienkaemper, J. J., P. L. Williams, and T. P. Guilderson (2010). Evidence for a 12th large earthquake on the southern Hayward fault in the past 1900 years, *Bull. Seismol. Soc. Am.* **100**, 2024–2034.
- Louderback, G. D. (1947). Central California earthquakes of the 1830's, *Bull. Seismol. Soc. Am.* **37**, 33–74.
- Manighetti, I. M., M. Campillo, P. M. Mai, and G. King (2005). Evidence for self-similar, triangular slip distribution earthquakes: Implications for earthquake and fault mechanics, *J. Geophys. Res.* **110**, no. B05409, doi: [10.1029/2004JB003174](https://doi.org/10.1029/2004JB003174).
- McFarland, F. S., J. J. Lienkaemper, S. J. Caskey, and K. Grove (2007). Data from theodolite measurements of creep rates on San Francisco Bay region faults, California: 1979–2007, *U.S. Geol. Surv. Open-File Rept. 07-1367*, 111 pp.
- Mensing, S., and R. Byrne (1998). Pre-mission invasion of *Erodium cicutarium* in California, *J. Biogeogr.* **25**, 757–762.
- Niemi, T. M., H. Zhang, S. Generaux, and T. Fumal (2004). A 2500-year record of large earthquakes along the northern San Andreas fault at the Vedanta marsh, Olema, CA, in *Proceedings of the First Annual Northern California Earthquake Hazards Workshop*, M. L. Zoback (Editor), 13–14 January 2004, USGS Open File Rept. 2004-1424, 74 pp.
- Parsons, T. (2002). Post-1906 stress recovery of the San Andreas fault system calculated from 3-D finite element analysis, *J. Geophys. Res.* **107**, ESE 3-1–ESE 3-13.
- Pollitz, F. R., and D. P. Schwartz (2008). Probabilistic seismic hazard in the San Francisco Bay area based on a simplified viscoelastic-cycle, *J. Geophys. Res.* **113**, no. B05409, doi: [10.1029/2007JB005227](https://doi.org/10.1029/2007JB005227).
- Prentice, C. S., and D. P. Schwartz (1991). Re-evaluation of 1906 surface faulting, 888 geomorphic expression, and seismic hazard along the San Andreas fault in the 889 southern Santa Cruz Mountains, *Bull. Seismol. Soc. Am.* **81**, 1424–1479.
- Reasenber, P. A., T. C. Hanks, and W. H. Bakun (2003). An empirical model for earthquake probabilities in the San Francisco Bay region, California, *Bull. Seismol. Soc. Am.* **93**, 1–13.
- Reid, H. F. (1910). The Mechanics of the Earthquake, The California Earthquake of April 18, 1906, *Report of the State Investigation Commission*, 2, Carnegie Institution of Washington, Washington, D.C., 16–28.
- Reidy, L. M. (2001). Evidence of environmental change over the last 2000 years at Mountain Lake, in the northern San Francisco Peninsula, California, *M.A. Thesis*, University of California, Berkeley, 108 pp.
- Schwartz, D. P. (2006). A look back at 1906—Perspectives on great earthquakes and post-earthquake investigations, *Seismol. Res. Lett.* **77**, 123–127.
- Schwartz, D. P., P. H. Haeussler, G. G. Seitz, and T. E. Dawson (2012). Why the 2002 Denali fault rupture propagated onto the Totschunda fault: Implications for fault branching and seismic hazards, *J. Geophys. Res.* **117**, no. B11304, doi: [10.1029/2011JB008918](https://doi.org/10.1029/2011JB008918).
- Schwartz, D. P., D. Pantosti, S. Hecker, K. Okumura, K. E. Budding, and T. Powers (1992). Late Holocene behavior and seismogenic potential of the Rodgers Creek fault zone, Sonoma County, California, in G. Borchardt, S. E. Hirschfeld, J. J. Lienkaemper, P. McClellan, and I. G. Wong (Editors), *Proc. of the Second Conference on Earthquake Hazards in the Eastern San Francisco Bay Area*, Calif. Div. Mines Geol. Spec. Publ., 113, 393–398.
- Schwartz, D. P., D. Pantosti, K. Okumura, T. J. Powers, and J. Hamilton (1998). Paleoseismic investigations in the Santa Cruz Mountains, CA: Implications for recurrence of large magnitude earthquakes on the San Andreas fault, *J. Geophys. Res.* **103**, 17,985–18,001.
- Sieh, K. E. (1978). Slip along the San Andreas fault associated with the great 1857 earthquake, *Bull. Seismol. Soc. Am.* **68**, 1421–1448.
- Simpson, G. D., and K. L. Knudsen (2000). Paleoseismic investigation of the northern San Gregorio fault at the Pillar Point Marsh near Half Moon Bay, California, Final Technical Report submitted to U.S. Geological Survey Western Region, Bay Area Paleoseismological Experiment (BAPEX), Contract Number 98WRCN1012, CLIN0014, 34 pp.
- Simpson, G. D., J. N. Baldwin, K. I. Kelson, and W. R. Lettis (1999). Late Holocene slip rate and earthquake history for the northern Calaveras fault at Welch Creek, eastern San Francisco Bay area, California, *Bull. Seismol. Soc. Am.* **89**, 1250–1263.
- Simpson, G. D., S. C. Thompson, J. S. Noller, and W. R. Lettis (1997). The northern San Gregorio fault zone: Evidence for the timing of late Holocene earthquakes near Seal Cove, California, *Bull. Seismol. Soc. Am.* **87**, 1158–1170.
- Simpson, R. W., and P. A. Reasenber (1994). Earthquake-induced static stress changes on central California faults, in *The Loma Prieta, California, Earthquake of October 17, 1989—Tectonic Processes and Models*, U.S. Geol. Surv. Prof. Pap. 1550-F, 55–89.
- Sims, J. D. (1993). Parkfield area tectonic framework [abs.], in *Summaries of Technical Reports*, M. L. Jacobson (Editor), Vol. XXXIV, Prepared by participants in the National Earthquake Hazards Reduction Program, *U.S. Geol. Surv. Open-File Rept. 93-195*, 682–684.
- Song, S. G., G. C. Beroza, and P. Segall (2008). A unified source model for the 1906 San Francisco earthquake, *Bull. Seismol. Soc. Am.* **98**, 823–831.
- Streig, A. R., T. E. Dawson, and R. J. Weldon II (2014). Paleoseismic evidence of the 1890 and 1838 earthquakes on the Santa Cruz Mountains section of the San Andreas fault, near Corralitos, CA, *Bull. Seismol. Soc. Am.* **104**, 285–300, doi: [10.1785/0120130009](https://doi.org/10.1785/0120130009).
- Sykes, L. R., and S. C. Jaume (1990). Seismic activity on neighboring faults as a long-term precursor to large earthquakes in the San Francisco Bay area, *Nature* **348**, 595–599.
- Sykes, L. R., and S. P. Nishenko (1984). Probabilities of occurrence of large plate rupturing earthquakes for the San Andreas, San Jacinto, and Imperial faults, California, 1983–2003, *J. Geophys. Res.* **89**, 5905–5927.
- Thatcher, W., G. Marshall, and M. Lisowski (1997). Resolution of fault slip along the 470-km-long rupture of the great 1906

- San Francisco earthquake and its implications, *J. Geophys. Res.* **102**, 5353–5367.
- Tocher, D. (1959). Seismic history of the San Francisco region, in San Francisco Earthquakes of 1957, *Calif. Div. Mines Geol. Spec. Rept.* **57**, 39–48.
- Topozada, T. R., and G. Borchardt (1998). Re-evaluation of the 1836 “Hayward Fault” and the 1838 San Andreas earthquakes, *Bull. Seismol. Soc. Am.* **88**, 140–159.
- Topozada, T. R., C. R. Real, and D. L. Parke (1981). Preparation of iso-seismal maps and summaries of reported effects for pre-1900 California earthquakes, *Calif. Div. Mines Geol. Open-File Rept. 81-11 SAC*, 182 pp.
- Townley, S. D., and M. W. Allen (1939). Descriptive catalog of earthquakes of the Pacific coast of the United States 1769 to 1928, *Bull. Seismol. Soc. Am.* **29**, 1–297.
- Tuttle, M. P., and L. R. Sykes (1992). Re-evaluation of several large historic earthquakes in the vicinity of the Loma Prieta and peninsular segments of the San Andreas fault, California, *Bull. Seismol. Soc. Am.* **82**, 1802–1820.
- Wald, D. W., H. Kanamori, D. V. Helmlinger, and T. H. Heaton (1993). Source study of the 1906 San Francisco earthquake, *Bull. Seismol. Soc. Am.* **83**, 981–1019.
- Wells, D. L., and K. J. Coppersmith (1994). New empirical relationships among magnitude, rupture length, rupture width, rupture area, and surface displacement, *Bull. Seismol. Soc. Am.* **84**, 974–1002.
- Wesnousky, S. G. (2008). Displacement and geometrical characteristics of earthquake surface ruptures: Issues and implications for seismic hazard analysis and the process of earthquake rupture, *Bull. Seismol. Soc. Am.* **98**, 1609–1632.
- Wesson, R. L., W. H. Bakun, and D. M. Perkins (2003). Association of earthquakes in San Francisco Bay area using Bayesian inference, *Bull. Seismol. Soc. Am.* **93**, 1306–1332.
- Working Group on California Earthquake Probabilities (WGCEP) (1988). Probabilities of large earthquakes occurring in California, *U.S. Geol. Surv. Open-File Rept. 88-398*, 62 pp.
- Working Group on California Earthquake Probabilities (WGCEP) (1990). Probabilities of large earthquakes in the San Francisco Bay region, California, *U.S. Geol. Surv. Circ. 1053*, 51 pp.
- Working Group on California Earthquake Probabilities (WGCEP) (1999). Earthquake probabilities in the San Francisco Bay region: 2000–2030, *U.S. Geol. Surv. Open-File Rept. 99-517*, 55 pp.
- Working Group on California Earthquake Probabilities (WGCEP) (2003). Earthquake probabilities in the San Francisco Bay region: 2002–2031, *U.S. Geol. Surv. Open-File Rept. 03-214*, 235 pp., <http://pubs.usgs.gov/of/2003/of03-214/> (last accessed August 2013).
- Working Group on California Earthquake Probabilities (WGCEP) (2008). The uniform California earthquake rupture forecast, *U.S. Geol. Surv. Open-File Rept. 2007-1437*, <http://pubs.usgs.gov/of/2007/1437/> (last accessed August 2013).
- Yu, E., and P. Segall (1996). Slip in the 1868 Hayward earthquake from the analysis of historical triangulation data, *J. Geophys. Res.* **101**, 16,101–16,118.
- Zhang, H. (2005). Paleoseismic studies of the northern San Andreas fault at Vedanta Marsh site, Olema, California, *Ph.D. dissertation*, University of Missouri-Kansas City, Kansas City, 334 pp.
- Zhang, H., T. Niemi, and T. Fumal (2006). A 3000-year record of earthquakes on the northern San Andreas fault at the Vedanta Marsh site, Olema, California, *Seismol. Res. Lett.* **77**, 176.
- Zielke, O., R. J. Arrowsmith, L. Grant Ludwig, and S. O. Akçiz (2010). Slip in the 1857 and earlier large earthquakes along the Carrizo Plain, San Andreas fault, *Science* **327**, 1119–1122.

turing earthquakes in the San Francisco Bay Region (SFBR) since ~1600. Surface ruptures that produce large moment-releasing earthquakes typically leave their signature at the surface. This is recorded as disruption of the stratigraphy exposed in trenches excavated across the faults. Paleoseismic dates for the SFBR primarily rely on the use of radiocarbon dating, with the most commonly available organic material being detrital charcoal. A single sample provides a mean age of the sample and a counting uncertainty. This, in turn, is dendrochronologically calendar corrected to provide the full possible age range of the sample, which is represented by a probability density function (PDF). The ideal field situation is the occurrence of datable deposits immediately below and above a rupture event horizon, but even here the uncertainties in the age ranges of these units can be broad. By using radiocarbon PDFs for each horizon, the probability distribution can be trimmed and reweighted using a radiocarbon calibration program such as OxCal (Bronk Ramsey, 2001, 2007; Lienkaemper and Bronk Ramsey, 2009). The result, generally, is a tighter distribution from which a mean date of the event and  $1\sigma$  and  $2\sigma$  uncertainty ranges can be extracted. For many radiocarbon samples formed in the seventeenth and eighteenth centuries, the age-range probabilities can extend well into the nineteenth and/or twentieth centuries. This is a potential problem for estimating the ages of the relatively young paleoseismic earthquakes considered here, particularly where a rupture offsets a dated horizon and there is no unfaulted overlying deposit or the postevent deposit is not datable. For this reason the founding of the Mission Dolores and Presidio provides a major time constraint that allows radiocarbon PDFs to be truncated at 1776.

In addition to radiocarbon, the presence or absence of non-native pollen (Mensing and Byrne, 1998; Reidy, 2001) has provided a basis for event dating at some locations. Of particular importance is *Erodium cicutarium*, a non-native pollen that first appeared in the SFBR about 1770 and was ubiquitous in the region by 1800. The presence or absence of this pollen in critical deposits plays an important role in dating SFBR paleoseismic earthquakes that occurred between the mid-late 1700s and early-middle 1800s.

The occurrence and dating of post-1600 earthquakes are described below. For long faults such as the San Andreas and Hayward–Rodgers Creek, where either absence of observations or overlapping radiocarbon dates at different localities permit alternative rupture histories, we present these alternatives. Sites where event ages have been obtained are shown in Figure 2. The mean paleoseismic dates and  $2\sigma$  age ranges are listed in Table 2 and shown graphically in Figure 3. All dates given in the following discussions, figures, and tables are in A.D. The description of faults and fault segments follows the nomenclature developed by Working Group on California Earthquake Probabilities (WGCEP) (2003) and shown in Figures 1 and 2.

## Appendix A

### Dating the Recent Surface Ruptures

This appendix provides detail of the observations and analyses that are used to develop the chronology of the surface-ruptures

### San Andreas Fault

The San Andreas fault is the dominant active structural element in the SFBR. It has the highest slip rate and

consequently releases the largest amount of seismic moment of any earthquake source in the region. The 1906 rupture extended approximately 470 km from Shelter Cove on the north to San Juan Bautista on the south. An important issue is the degree to which the fault fails in repeats of the 1906 rupture or as shorter ruptures. Investigations to provide the timing of paleoearthquakes have varied in their success. Gaps in information exist for the timing of events, particularly along the San Francisco Peninsula and the northern Santa Cruz Mountains, and alternative rupture scenarios can be entertained. [Schwartz \*et al.\* \(1998\)](#) conclude that a large, long 1906-type rupture likely occurred between 1600 and 1670. They estimated the timing and length of this event based on then-available radiocarbon dating of trench relations reported at five locations along the 1906 rupture between the southern Santa Cruz Mountains and Point Arena (Arano Flat, Grizzly Flats, Dogtown, Vedanta, Point Arena; Fig. 2). This event was also identified at Tomales Bay and Bolinas Lagoon ([Knudsen \*et al.\*, 2002](#)). [Schwartz \*et al.\* \(1998\)](#) do not exclude the possibility of shorter closely timed events on different segments of the fault within the radiocarbon uncertainties, and this may be the case for the proposed 1600–1670 event. More recent paleoearthquake chronologies discussed below suggest that, in fact, the San Andreas likely fails more frequently as shorter (though still long) segments, as opposed to full ruptures (such as in 1906). We use the observations below in interpreting the post-1600 event chronology.

#### San Andreas North Coast (SAN) and San Andreas Offshore Segments

Between the Golden Gate and Point Arena, on the section of the fault referred to as the North Coast segment, estimates of the timing of pre-1906 surface ruptures have been developed at eight locations. [Kelson \*et al.\* \(2006\)](#) summarize event ages at six of these in their discussion of the Fort Ross Orchard site (see below). Subsequently, additional timing of paleoearthquakes has been reported at the Vedanta Marsh ([Zhang, 2005](#)) and Dogtown ([Hall and Niemi, 2008](#)) sites. The present discussion focuses on the results at three of the sites on land (Fort Ross Orchard, Vedanta Marsh, and Dogtown). At these locations, OxCal radiocarbon models have been developed by the respective site investigators. North of Point Arena, the fault extends offshore as the San Andreas Offshore (SAO) segment, emerging 150 km to the north at Shelter Cove. Along the offshore segment of the fault, as well as along the North Coast segment, the mapping and dating of turbidites ([Goldfinger \*et al.\*, 2007, 2008](#)) provide estimates of dates of paleoearthquakes.

[Kelson \*et al.\* \(2006\)](#) excavated trenches across an uphill-facing scarp that defines the San Andreas fault at the Fort Ross Orchard site (Fig. 2). The trenches exposed colluvial deposits adjacent to the fault that were interpreted as being derived from a degrading fault scarp produced by the penultimate and prepenultimate surface ruptures. Based on dating

of detrital charcoal from deposits within the colluvium that interfinger with wash deposits from the opposite slope, they obtained a  $2\sigma$  age range of 1660–1812 for the penultimate event. The 1812 date reflects their use of the Russian settlement of Fort Ross as a constraint. We think it is likely that a large rupture at Fort Ross and at locations to the south would have been recorded earlier and use 1776. At the Vedanta Marsh (Fig. 2), which contains a slowly accumulating sequence of silts, sands, and peats, [Niemi \*et al.\* \(2004\)](#) presented a preliminary chronology of 11 paleoearthquakes in the past ~2660 years and interpreted the timing of the penultimate surface rupture as occurring between 1680 and 1790. In a highly detailed description of faulting and stratigraphy at the Vedanta Marsh, [Zhang \(2005\)](#) and [Zhang \*et al.\* \(2006\)](#) present alternative interpretations for the timing of the penultimate event, depending on whether the rupture stopped within or extended to the top of a stratigraphic horizon designated unit 10. With the rupture extending to the top of the unit, which is the preferred model ([Zhang, 2005](#)), the penultimate event occurred between 1680 and 1740. If the rupture extended only to the middle of the horizon, the event would have occurred between 1510 and 1640. Fifteen kilometers to the south of Vedanta, at the Dogtown site, [Hall and Niemi \(2008\)](#) combined observations from earlier paleoseismic investigations ([Hall, 1981](#); [Cotton \*et al.\*, 1982](#)) with more recent trenching. They interpret the occurrence of the penultimate northern San Andreas rupture based on the presence of fissure infills and upward-terminating faults in deposits immediately below a gravel that was only offset by the 1906 event. Their OxCal modeling of radiocarbon dating of detrital charcoal constrains the age of the penultimate rupture between 1695 and 1776.

Based on offshore coring, [Goldfinger \*et al.\* \(2007\)](#) identified and correlated 15 turbidites between Noyo Channel and Pioneer Channel (a distance of approximately 270 km; Fig. 1) that formed during the past 2800 years. [Goldfinger \*et al.\* \(2007\)](#) interpreted the turbidites as earthquake triggered, based on four observations: (1) individual turbidites extend over long distances; (2) 1906 shaking triggered turbidities that can be seen in the cores; (3) the average interval between the past 15 turbidities is approximately 200 ( $\pm 60$ ) years, which is in reasonable agreement with the average land interval of 248 ( $\pm 15$ ) years for the past 11 ruptures at Vedanta ([Zhang \*et al.\*, 2006](#)); and (4) the calculated age of each of the five most recent is generally coincident with paleoearthquakes dated on land. They suggest the along-strike correlation of 11 out of the 15 most recent turbidities indicates the northern San Andreas ruptured from the Mendocino triple junction to at least the vicinity of San Francisco. This would include the Offshore and North Coast segments of the San Andreas fault. Based on radiocarbon dating of foraminifera and analysis of sedimentation rates, ([Goldfinger \*et al.\*, 2007, 2008](#)) calculate the penultimate turbidite formed between 1647 and 1819, with a preferred date of 1724. By combining this turbidite age range with the on-land Vedanta and Fort Ross dates and truncating the distribution with the date of

San Francisco mission construction (given, without discussion, as 1769 as opposed to 1776), [Goldfinger \*et al.\* \(2008\)](#) conclude the penultimate earthquake occurred between 1700 and 1750.

#### Peninsula San Andreas

This section of the San Andreas fault, as defined by [WGCEP \(1999, 2003\)](#) extends approximately 85 km from the Golden Gate to the north end of the Santa Cruz Mountains near Los Gatos (Fig. 2). There are no well-constrained geologic observations for either the historical or paleoseismic record, and the Peninsula San Andreas (SAP) presents a major gap in the Bay Area earthquake history. The historical 1838 earthquake has been attributed to this section of the San Andreas ([Louderback, 1947](#); [WGCEP, 1988, 1990](#)). [Sykes and Nishenko \(1984\)](#), [Tuttle and Sykes \(1992\)](#), and [Topozada and Borchardt \(1998\)](#) compared intensity observations at Monterey from the 1838, 1906, and 1989 (Loma Prieta) earthquakes, and all conclude that the 1838 rupture extended from the San Francisco Peninsula into the Santa Cruz Mountains and possibly as far south as San Juan Bautista. [Tuttle and Sykes \(1992\)](#) estimated a magnitude of  $M \geq 7.2$ , and [Topozada and Borchardt \(1998\)](#) estimated an  $M \sim 7.5$ . [Bakun \(1999\)](#) presents a thorough discussion of these issues. Using the same intensity reports, [Bakun \(1999\)](#) interprets the Peninsula segment as a high-probability source for the earthquake but estimates a smaller magnitude of  $M$  6.8 ( $M$  6.3–7.2 at 95% confidence range).

Geological studies have yet to show conclusively whether the 1838 earthquake was or was not produced by rupture of the SAP. [Hall \*et al.\* \(1999\)](#) reconstructed buried stream channels offset by the San Andreas fault at the Filoli site (Fig. 2). They conclude that a channel with a radiocarbon age of  $330 \pm 200$  years B.P. is offset to  $4.1 \pm 0.5$  m. This is interpreted as recording 2.5 m ( $\pm 0.2$ ) of surface slip that occurred at this location in 1906 and  $1.6 \pm 0.7$  m of slip in the penultimate rupture, which they contend is 1838. Although the 1.6 m mean offset is consistent with the [Bakun \(1999\)](#) magnitude suggested for 1838, the radiocarbon dating provides no absolute constraint. Based on these observations, we assign the 1838 event to the SAP, noting that there is significant uncertainty in this interpretation.

A possible earlier rupture is even less clear. [Hall \*et al.\* \(1999\)](#) identify fault-parallel channels in the Filoli trenches. They speculate that these channels, in contrast to those that cross the fault, likely formed in response to local topography produced by the rupture that diverted channel flow. Although this interpretation is permissive, it is highly uncertain. Based on the radiocarbon dating of detrital charcoal from one of the fault-parallel channels, [Hall \*et al.\* \(1999\)](#) conclude that they formed within or slightly after the interval of 1450–1670.

#### Santa Cruz Mountains Segment (SAS)/San Juan Bautista Segment

The Santa Cruz Mountains segment of the San Andreas, as defined by [WGCEP \(2003\)](#), extends 62 km ( $\pm 15$ ) from the north end of the Loma Prieta aftershock zone near Los Gatos to the south end of the 1906 rupture at San Juan Bautista. The Working Group placed a  $\pm 5$  km uncertainty on this southeast end point (Fig. 2). As originally defined, the segment includes the transition from a locked to a creeping section of the fault along its southern 15 km. [Johanson and Burgmann \(2005\)](#) use Global Positioning System and Interferometric Synthetic Aperture Radar data to propose a 46 km long transition zone from a locked to a fully creeping San Andreas fault, similar to the Parkfield transition zone, that they name the San Juan Bautista (SJB) segment. It extends from 16 km north of San Juan Bautista to 30 km south of it and encompasses the southern part of the [WGCEP \(2003\)](#) Santa Cruz Mountains segment. We have adopted this interpretation and modified the [WGCEP \(2003\)](#) segmentation to make a significantly longer (20 km) zone of uncertainty as to where ruptures associated with each segment are likely to extend (Figs. 1, 2).

[Johanson and Burgmann \(2005\)](#) suggest the San Juan Bautista segment is accumulating strain energy at the rate of one  $M$  6.3–6.7 per century. Because the southern boundary of our SFBR rectangle is located just south of San Juan Bautista, the overall area of the SJB segment does not affect seismic moment in our analysis, but its modeled rupture behavior has implications for interpretation of paleoseismic observations. The timing of surface ruptures since 1600 for the Santa Cruz Mountains and San Juan Bautista segments of the San Andreas fault relies on observations at Grizzly Flats ([Schwartz \*et al.\*, 1998](#)), Mill Canyon ([Fumal, Dawson, \*et al.\*, 2004](#); [Fumal, 2012](#)), Arano Flat ([Fumal \*et al.\*, 2003](#); [Fumal, Heingartner, Samrad, \*et al.\*, 2004](#)), and Hazel Dell ([Streig \*et al.\*, 2014](#)) (Fig. 2). Grizzly Flats is located 16 km north of the transition from creeping to locked fault, and Hazel Dell is 10 km to the north of it. The Mill Canyon and Arano flat sites are located 2 km and 1 km, respectively, north of the transition (Fig. 2).

At Grizzly Flats, [Schwartz \*et al.\* \(1998\)](#) interpreted a series of alluvial sands and silts deposited since the mid-1660s to be offset, within the resolution of the trench exposures, by only the 1906 rupture. The oldest unit in this stratigraphic sequence is dated at 1640–1659 with 100% of the probability within this range. This unusually tight range was obtained by combining the ages of all samples in the deposit to calculate a weighted mean age, and then calibrating the weighted mean. This method ([Gillespie, 1984](#)) resulted in a large reduction in the sample age uncertainty and the ensuing narrow age range for the deposit (averaging of radiocarbon dates is not presently used in OxCal modeling). The age of the penultimate event is not directly constrained by subsurface observations at Grizzly Flats. [Jacoby \(1995\)](#) identified a redwood stump located on the

fault just south of the Grizzly Flats trenches. His analysis of a tree-ring core obtained from the stump showed wide tree rings just prior to an abrupt decrease in ring width. [Jacoby \(1995\)](#) interprets the growth change to be the result of surface rupture affecting the tree. He dated the wide rings at  $220 \pm 50$  yr B.P., which yielded a preferred  $2\sigma$  range of 1632–1822. [Schwartz et al. \(1998\)](#) combined the trench and tree-ring observations and placed the penultimate rupture between 1632 and 1659. They note that, because of analytic and stratigraphic uncertainties, the interval may be too narrow and refer to the penultimate event as a mid-1600s earthquake. With current calibration curves such as Calib 7.0 (see [Data and Resources](#)), the original radiocarbon date of the tree rings yields a  $2\sigma$  age range of 1520–1592 (0.085), 1619–1700 (0.315), 1703–1705 (0.001), 1727–1819 (0.425), 1832–1880 (0.048), and 1915–1950 (0.126).

The Mill Canyon and Arano Flat sites, 15.0 and 16.0 km south of Grizzly Flats (Fig. 2), respectively, have a combined paleoseismic record that shows evidence of at least nine ruptures during the past approximately 1000 years ([Fumal et al., 2003](#); [Fumal, Dawson, et al., 2004](#); [Fumal, Heingartner, Samrad, et al., 2004](#)). At Mill Canyon ([Fumal, 2012](#)), the most recent surface-rupturing event is the 1906 San Francisco earthquake, and it is well expressed as a series of in-filled fissures and small scarps. In addition to that of 1906, evidence was found for three surface-rupturing earthquakes since about 1500. Radiocarbon ages of detrital charcoal suggest an age of the penultimate earthquake of 1711–1770, with a mean date of 1750. Support for this age comes from a 1.5 m deep fissure that formed during this earthquake. It was sampled for *Erodium* pollen, which was not found and would have been present at this site in 1838 in the fill of any fissure formed during an earthquake of that vintage ([Fumal, Heingartner, Samrad, et al., 2004](#)). [Fumal \(2012\)](#) favors this interpretation but also offers an alternative model for this event of 1789–1904, suggesting that it could be either the 1838 or 1865 SFBR earthquakes. The prepenultimate rupture at Mill Canyon was initially dated between 1600 and 1680, with a mean date of this rupture at 1640 ([Fumal, Dawson, et al., 2004](#)) and revised to 1660–1720 with a mean date of 1690 ([Fumal, 2012](#)). Additionally, [Fumal \(2012\)](#) uses OxCal to model the radiocarbon dates from Grizzly Flats and presents his own structural interpretation of the trench logs. He suggests that in addition to the 1906 event, there could be two other ruptures, one of which correlates with the penultimate event at Mill Canyon.

At Arano Flat, faulting is expressed as a 1–2 m wide zone that deforms alluvial fan deposits overlying well-bedded stream overbank deposits. The trenches at this location were interpreted to contain evidence for at least nine surface-faulting earthquakes since about 1000 ([Fumal, Dawson, et al., 2004](#); [Fumal, Heingartner, Samrad, et al., 2004](#)). Evidence for ground-rupturing events includes in-filled fissures, folding with growth strata, and multiple upward terminations of fault traces. Subsequent to the investigations noted above, additional OxCal modeling of dates was undertaken (T. Fumal, written comm., 2010), which dated the penultimate rupture

at Arano Flat between 1721 and 1785 ( $2\sigma$ ), with a mean date of 1753. This appears to be the same event as Mill Canyon. For the third event back at Arano Flat, the revised analysis dates the rupture at 1624 with a  $2\sigma$  age range of 1584–1659.

[Streig et al. \(2014\)](#) excavated trenches across the San Andreas fault at the Hazel Dell site, 6 km south of Grizzly Flats. They report the occurrence of four surface-faulting events through a sequence of stream overbank deposits. On the basis of wood chips in their unit 400a, which are interpreted as being axe cut, and historical review of the redwood logging history of that area, they interpret the three most recent events as historical, with the prepenultimate being the rupture from the 1838 earthquake. They conclude that a younger rupture represents the 1890 earthquake, for which surface rupture is known at San Juan Bautista ([Lawson, 1908](#)) and at least 3 km to the north of it ([Prentice and Schwartz, 1991](#)). The most recent event is 1906. With this working chronology, [Streig et al. \(2014\)](#) reinterpret the event chronology at Arano Flat and Mill Canyon to include 1838 and 1890 and suggest that at least the 1838 rupture is present at Grizzly Flats.

#### San Andreas: Summary

Significant effort has been spent on obtaining dates of paleoearthquakes along the 1906 rupture of the San Andreas fault. On the North Coast segment, there appears to be a convergence of dating estimates from multiple sites, including from offshore turbidite analysis, which indicates there has been one large surface rupture along it between 1660 and 1776. Two-sigma age ranges at three land sites (and from offshore) indicate the rupture did not occur earlier than 1660 and suggest a more likely occurrence time in the 1700s. There does not appear to be a statistical basis for specifying a mean date for the event, and we place it at the midpoint of the range, which is 1735.

The Peninsula segment of the San Andreas fault remains an enigma and a data gap. As discussed, we assign the 1838 event to the Peninsula San Andreas, noting that there is significant uncertainty in this interpretation. There is no firm basis at present to identify, let alone date, older events on the Peninsula. Based on radiocarbon dating of detrital charcoal from a fault-parallel channel that may have been diverted by surface faulting, [Hall et al. \(1999\)](#) suggest that an event occurred within or slightly after the 1450–1670 interval. Even if the interpretation is correct, the range is highly unconstrained, although we place a tentative date of 1600 (shown as a dashed line) to allow for the possibility of its occurrence as part of the maximum source model (Fig. 3b).

For most of the length of the Santa Cruz Mountains segment, there are no paleoseismic data. The evolving and alternative interpretations of both timing and extent of rupture at its southern end, at or near the transition to the creeping San Juan Bautista segment, are summarized above. The effects of these alternatives on the moment sums and moment rates developed in the present paper are noted here. If the 1838 rupture is at Hazel Dell and it extended onto the Peninsula

segment, [Streig \*et al.\* \(2014\)](#) suggest an  $M \sim 7$  (6.8–7.2) for the earthquake. With regard to the moment release calculations, which use an  $M$  6.8 (mean magnitude of [Bakun, 1999](#)), the effect would be to increase the  $\Sigma M_0/\text{yr}$  for the postcluster interval (1777–1905) by 13% and to increase the  $\Sigma M_0/\text{yr}$  for the 1600–2012 interval by less than 2%. There is also the possibility, though quite small, that the earthquake of 1836 ( $M$  6.5 [5.9–7.0]; [Bakun, 1999](#)), which is very poorly located but is suggested to be east of Monterey Bay ([Topozada and Borchardt, 1998](#); [Bakun, 1999](#)), could have occurred on the San Juan Bautista segment and ruptured into the southern Santa Cruz Mountains. The moment for the 1836 event is incorporated into the present SFBR analysis as part of the historical moment release estimate of [Bakun \(1999\)](#).

The 1890 earthquake has an estimated magnitude of  $M$  6.3 (6.0–6.5) ([Bakun, 1999](#)). The nucleation location is uncertain. However, because surface rupture of the San Andreas fault is documented on the creeping section in San Juan Bautista and just to the northwest of it, we have preferentially assigned the event to the San Juan Bautista segment. The seismic moment of the 1890 earthquake is incorporated into the current moment release rate analysis within the historical moment release estimate of [Bakun \(1999\)](#).

In modeling the SFBR earthquake cycle, a 1750 earthquake on the San Juan Bautista segment is included in the 1690–1776 cluster. This was considered a San Juan Bautista event, based on the timing of the penultimate event at Arano Flat and Mill Canyon (summarized above) and the interpretation of [Schwartz \*et al.\* \(1998\)](#) that only the 1906 event occurs in the younger Grizzly Flats record. Although they note the timing on one of the four fault traces in the trenches is not constrained and while an additional slip event on this trace is permissive, there is no evidence that it occurred. If this rupture is actually the 1838 earthquake, 1750 would be removed from the cluster. Because only a limited length of the San Juan Bautista segment is in the SFBR box, the moment contribution from this event is small (Table 5) and is less than 1% of the total moment of the 1690–1776 cluster (Table 6).

We use the 1624 date at Arano Flat to represent the penultimate Santa Cruz Mountains segment rupture. This is consistent with the interpretations at Grizzly Flats, including at least part of the tree-ring age probability. Extending this rupture as far north as Filoli is permitted, but this is poorly constrained. However, we have included this as an alternative rupture possibility (Fig. 3b), in part to show the important effect of a full Peninsula/Santa Cruz Mountains rupture on SFBR moment release.

### Hayward Fault

The Hayward fault extends 85 km from the approximately 6 km wide Rodgers Creek extensional fault step over in San Pablo Bay on the north to the Warm Springs district of Fremont on the south (Fig. 1). The fault has been divided into southern and northern segments ([WGCEP, 1999, 2003](#)) on

the basis of the geodetically measured extent of the 1868 rupture, which appears to have terminated north of Berkeley ([Yu and Segall, 1996](#)), leaving the northern  $\sim 30$  km of the fault unruptured in this event. However, this segmentation may not represent the general long-term behavior of the fault. It is not certain that the northern Hayward fault (HN, Fig. 1) has the ability to repeatedly rupture independently to produce large earthquakes because of the depth extent of creep ([Bürgmann \*et al.\*, 2000](#); [Lienkaemper \*et al.\*, 2012](#)). We retain the north–south nomenclature but note that full fault ruptures, possibly controlled by an  $\sim 50$  km long asperity ([Lienkaemper \*et al.\*, 2012](#)), may be more typical. The Hayward fault has been probed repeatedly with trenches, but it has only yielded timing of past ruptures at two locations. These are the Tyson’s Lagoon site on the southern Hayward and the Mira Vista site on the northern segment (Fig. 2).

### Southern Hayward Fault

Evidence for 11 coseismic ruptures between A.D. 136 and 1868 has been found in a continuous stratigraphic sequence at the Tyson’s Lagoon (also called the Tule Pond) site ([Lienkaemper \*et al.\*, 2002](#); [Lienkaemper and Williams, 2007](#); [Lienkaemper \*et al.\*, 2010](#)) (Fig. 2). Tyson’s Lagoon is a large sag pond in a right step along the fault that has been the location of deposition throughout the Holocene. Although the main trace of the fault is creeping, stratigraphic and structural relations allow coseismic slip to be distinguished from creep. A set of small-displacement faults, including a graben, occurs in a 3–5 m wide zone immediately east of the main trace and shows no evidence of creep. Within this zone, the upward terminations of individual fault strands at different stratigraphic horizons within the pond deposits and graben, and the occurrence of blocky colluvium derived from the formation of small fault scarps, are indicators of coseismic slip. Based on these relations, [Lienkaemper \*et al.\* \(2002\)](#) identified event horizons for the 1868 earthquake and the three previous ruptures. There have been three ruptures since 1600, including the 1868 earthquake. The penultimate event is defined by fault scarp colluvium along the main trace and progressive vertical slip and warping of sediment packages in the adjacent secondary zone. A revised OxCal model for the Tyson’s Lagoon sequence ([Lienkaemper and Williams, 2007](#)) places the mean date for the penultimate rupture at 1725, with a  $2\sigma$  age range of 1658–1786. The prepenultimate rupture, also identified by the occurrence of scarp colluvium, has a mean date of 1629, with a  $2\sigma$  range of 1537–1737.

### Northern Hayward Fault

The Mira Vista site is a small sag pond along the Hayward fault on what is now the second fairway of the Mira Vista golf course. Construction of the golf course began in 1912 and preserved the pond and its deposits. The earthquake event horizons interpreted in the trenches are based on displacements of finely bedded silts and sands by fault traces that are erosionally truncated and directly overlain by

unfaulted deposits (Hayward Fault Paleoseismicity Group, 1999). These faults with brittle slip and no apparent creep are immediately east of the main creeping trace in a structural setting similar to that adjacent to the main creeping trace at Tyson's Lagoon. The Hayward Fault Paleoseismicity Group (1999) interpreted a minimum of four to seven surface ruptures during the past 2400 years, acknowledging uncertainty in the completeness of the stratigraphic and earthquake record in the sag pond. However, evidence for the most recent event is among the best at this location. It is expressed by a fissure infill and five small (2–5 cm) individual vertical displacements of a stratigraphic contact, all of which are capped by unfaulted colluvium. The mean date of the most recent event at Mira Vista is 1705. The  $2\sigma$  age range is 1635–1776; the  $1\sigma$  range for this date is 1665–1776. The timing of the most recent event at the Mira Vista site and the penultimate event at the Tule Pond overlap and may very likely represent a rupture of the full Hayward fault.

#### Rodgers Creek Fault

The Rodgers Creek fault is a northern continuation of the Hayward fault. It extends 63 km ( $\pm 10$ ) from San Pablo Bay to about 10 km south of Healdsburg (Fig. 1). The fault has not produced a large historical rupture. The most recent large surface rupture is expressed as geomorphically fresh scarplets and short sections of mole track with left-stepping Reidel shears and extension fractures that occur intermittently along at least 35 km of the fault.

Paleoseismic trenches on the south-central reach of the Rodgers Creek (RC) fault at the Triangle G site (Fig. 2) provide the basis for dating the most recent surface rupture (Hecker *et al.*, 2005). These exposed both offset and unfaulted overbank and channel deposits that constrain the timing of the most recent large rupture. Using a range of charcoal sample ordering sequences, Hecker *et al.* (2005) ran four OxCal chronological models. With the 1776 Mission Dolores timing constraint at the younger end, these show that at  $2\sigma$  the most recent large rupture occurred no earlier than 1690. The preferred model places the most recent event at no older than 1715, with the probability distribution asymmetric and weighted toward the historical period. The mean date for the event is 1745. At  $1\sigma$ , the probability distribution begins at 1750. If the historical constraint is changed to 1824, the date of the founding of the nearby Sonoma Mission, 95% of the age distribution is no older than 1740. In addition non-native pollen is absent in the most recently faulted deposit and makes its first appearance in the overlying unfaulted units. This is consistent with the proposed mid-eighteenth century date.

The timing of the most recent event at the Triangle G site overlaps the timing of the most recent event at the Mira Vista site on the northern Hayward and the penultimate event on the southern Hayward at the Tyson's Lagoon, allowing the

possibility that both faults could have ruptured at the same time (WGCEP, 2003; Hecker *et al.*, 2005).

#### San Gregorio Fault

The San Gregorio (SG) fault extends from Monterey Bay on the south 110 km northward to a likely intersection with the San Andreas fault south of Bolinas Lagoon (Fig. 1). For two-thirds of its length, the fault is underwater, leaving few locations for obtaining paleoseismic data. The primary sites for the timing of past large earthquakes are at Seal Cove and Pillar Point Marsh (Fig. 2).

Initial investigation of the timing of paleoseismicity was undertaken by Simpson *et al.* (1997). They exposed evidence of the past two surface-faulting earthquakes in trenches excavated at Seal Cove. The most recent rupture offsets a Native American cooking hearth dated at 1270–1400. They conclude that it occurred within or more recently than a date in this range and 1775 (their stated arrival date of Spanish missionaries). Based on upward fault terminations in the trench exposures, Simpson *et al.* (1997) interpret the penultimate event to have occurred between 600 and 1400.

Pillar Point Marsh is a small graben along an extensional step in the SG fault 2.5 km south of Seal Cove (Fig. 2). Coring of the marsh deposits (Simpson and Knudsen, 2000) revealed a buried peat layer about 1.5 m below the present marsh surface. A sharp contact between the peat and overlying organic-poor mud, coupled with the presence of a fossil tidal flat diatom assemblage in the mud and a fresh water assemblage in deposits below the peat, led Simpson and Knudsen (2000) to conclude that the peat was buried as a result of rapid sea level change. They interpret this as coseismic subsidence during the most recent rupture of the SG fault, similar to what was observed at Bolinas Lagoon and Tomales Bay in 1906 (Knudsen *et al.*, 1997, 2002). Initial dating of the peat indicated burial between 1640 and 1776 ( $2\sigma$ ), with a possible shorter interval of 1685–1776.

Building on this, Koehler *et al.* (2005) conducted extensive additional coring of the marsh, as well as trenching at the north end. They found five buried peats in the marsh stratigraphy. Based on changes in diatom paleoecology, they conclude that tectonic subsidence has resulted in submergence of the Pillar Point Marsh and burial of peat soils (interpreted to represent former subareal marsh surfaces), two to four times during the past 4150–4410 cal yr B.P. The youngest peat (labeled "peat 1" on their fig. 6 and the same peat identified by Simpson and Knudsen, 2000) is found in all cores and is overlain across the entire marsh by a silty loam. The abrupt transition from fresh-brackish water diatoms in the peat to a low-marsh tidal flat environment in the loam indicates rapid sea level rise associated with submergence of the peat to a lower tidal level. Koehler *et al.* (2005) develop a set of criteria to rate the likelihood that each peat represents coseismic subsidence. This includes the presence of an abrupt lithologic contact, diatom evidence for abrupt sea

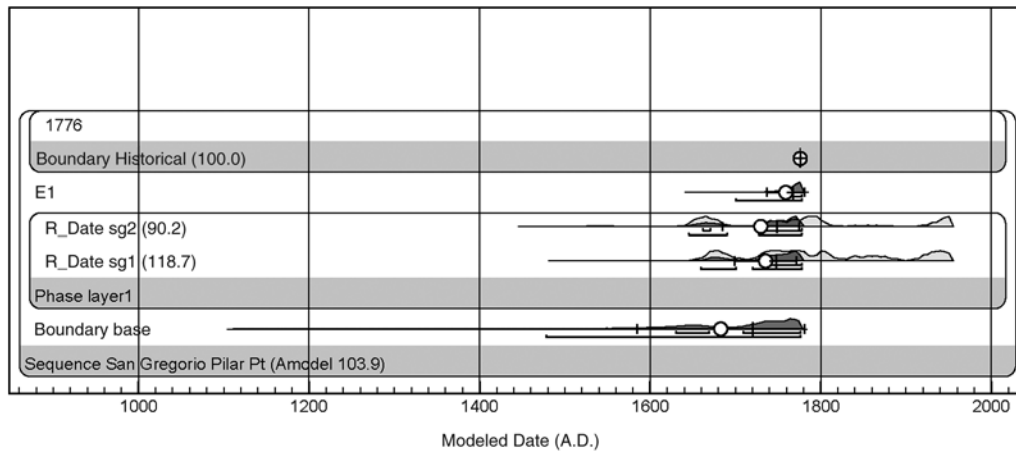


**Figure A1.** OxCal model (version 4.1.03) of the most recent event (R1) on the San Gregorio fault at Pillar Point Marsh.

level rise, evidence for sustained submergence and/or rapid aggradation, wide lateral extent of submergence, synchronicity with the timing of paleoseismic events at other locations, and being located close to an active fault. The upper peat satisfies all six, which leads [Koehler \*et al.\* \(2005\)](#) to conclude that, of all the peats in the marsh sequence, they have the highest confidence that it represents coseismic subsidence associated with the most recent rupture of the SG fault.

Seeds sampled by [Koehler \*et al.\* \(2005\)](#) from the upper peat gave radiocarbon ages of  $170 \pm 40$ ,  $210 \pm 40$ , and  $400 \pm 40$   $^{14}\text{C}$  cal yr B.P. We have run these radiocarbon dates through an OxCal chronological model. Using the 1776 historical constraint, the model gives an event age range of 1700–1776 ( $2\sigma$ ), with a mean date of 1759 (Fig. A1).

### Concord–Green Valley Fault

The Concord–Green Valley (CGV) fault is part of the easternmost fault system in the SFBR (Fig. 1). It extends a distance of approximately 130 km from Walnut Creek to northernmost Napa County. Large earthquakes have not occurred on the Concord–Green Valley fault historically. Initial paleoseismic investigation and trenching of the Green Valley fault was carried out by John Sims of the U.S. Geological Survey in 1991 at the Lopes Ranch site (Fig. 3). [Sims \(1993\)](#) interpreted the occurrence of three earthquakes based on offset alluvial deposits with thin organic horizons. More recent work at this location ([Baldwin \*et al.\*, 2008](#)) also identifies three paleoruptures. Although the fault is creeping at about 3–4 mm/yr ([McFarland \*et al.\*, 2007](#)), the presence of upward-flowering fault traces, steeply tilted alluvial fan deposits, upward fault terminations, and fissure fills indicate the deformation is primarily the result of coseismic slip ([Baldwin \*et al.\*, 2008](#)). The most recent rupture is expressed by offset and tilted fine sand and silt and a fissure infill, all overlain by unfaulted alluvium. Detrital charcoal from the youngest displaced stratigraphic unit and from the overlying unfaulted fan deposit was used as part of an OxCal model for the site. This yielded a mean date of  $1610 \pm 52$  yr and a  $2\sigma$

age range of 1511–1725, respectively (J. Baldwin and J. Lienkaemper, written comm., 2011). At the Mason Road site, 12 km north of Lopes Ranch (Fig. 2), [Lienkaemper \*et al.\* \(2013\)](#) obtained a similar age of  $1605 \pm 100$  yr, for the most recent paleorupture in a sequence of four surface-rupturing events that occurred since  $1013 \pm 32$  yr.

### Northern Calaveras Fault

The Northern Calaveras (CN) fault extends  $42 \pm 5$  km northwest from its transition from the creeping Central Calaveras (CC) fault ([Kelson, 2001](#); [WGCEP, 2003](#); [Kelson and Sundermann, 2007](#)) (Fig. 1). The current understanding of the late Holocene earthquake behavior of the CN fault is based primarily on data from the Leyden Creek and Welch Creek paleoseismic sites located near the southeast end of the segment (Fig. 2). Trench exposures at Leyden Creek and Welch Creek provide evidence for five or six surface ruptures in the past 2500 years, with an average recurrence of about 550 years and range in recurrence of 250–850 years ([Kelson \*et al.\*, 1996](#), [Simpson \*et al.\*, 1999](#)). Neither of these previous investigations, however, provides conclusive evidence addressing the timing of the most recent large earthquake. At both sites, fractures extend close to the present-day ground surface, but the ages of the youngest faulted deposit and the oldest unfaulted deposit are poorly constrained. [Kelson \*et al.\* \(1996\)](#) suggest the most-recent rupture may have occurred as much as 840 years ago, and [Simpson \*et al.\* \(1999\)](#) interpret the most-recent rupture as probably having occurred between 525 and 1295 years ago. Preliminary data from the Valley Crest Nursery site (Fig. 2) suggest that the most recent earthquake may have occurred prior to about A.D. 1570, and perhaps sometime between A.D. 1100 and 1300 ([Baldwin \*et al.\*, 1998](#)). Exploratory test pits and trenches at several other sites along the CN fault have not yielded well-constrained data on earthquake timing ([Kelson \*et al.\*, 2000a,b,c](#)). For example, the South Foothill site yielded evidence of large ruptures within the past 2500 years but no well-constrained event chronology ([Kelson and Randolph, 2000](#)).

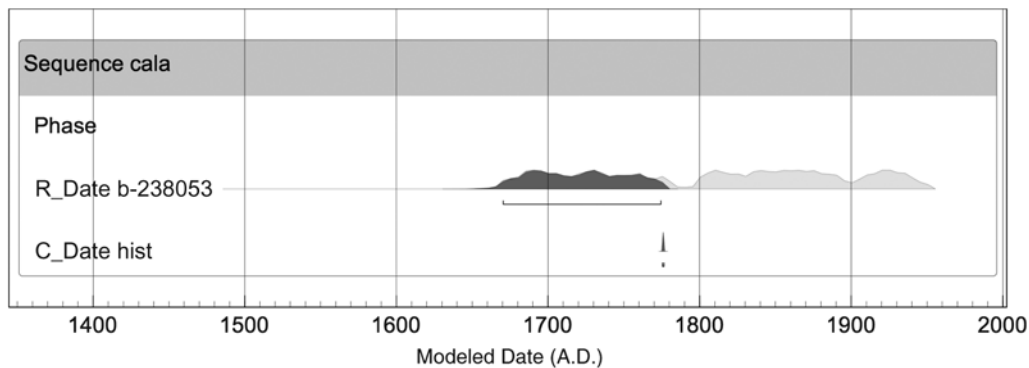


**Figure A2.** OxCal model (version 4.1.7) of the most recent event (R\_Date b-238053) on the northern Calaveras fault at the North Foothill site.

Research on the timing of ruptures on the CN fault occurred at the North Foothill site (Kelson *et al.*, 2008) (Fig. 2), which included multiple trench exposures containing a well-developed shear fabric that extends upward from the prominent bedrock fault zone and into prehistorical and historical deposits. Three distinct gravel-filled paleochannels are deformed within the fault zone, and evidence for recent surface rupture at this site is based on deformation of paleochannel deposits along a noncreeping, secondary reverse-oblique fault strand. Based on the trench exposures and limited age estimates from radiocarbon dating of detrital charcoal in the offset paleochannels, Kelson *et al.* (2008) conclude the most recent surface rupture along the CN fault appears to have occurred between 1660 and 1776. We have run the paleochannel radiocarbon date through OxCal (Fig. A2). This gives a mean date of 1740 and a  $2\sigma$  event range of 1692–1778, with the probability distribution skewed toward the historical period.

## Appendix B

### Observations of Paleo Offsets on SFBR Faults

#### San Andreas Fault

Large historical surface ruptures provide important calibration for recognizing and measuring offsets from prior ruptures, particularly at geomorphic piercing points such as gullies or small channels. The 1906 San Andreas rupture is estimated to have had a length of about 470 km (Thatcher *et al.*, 1997; Song *et al.*, 2008); however, about 60% occurred offshore. A review of the description of surface faulting documented in Lawson (1908) shows there are 36 locations, primarily fences and roads, where the amount of 1906 surface offset is reported or can be estimated; of these, only 20 are reliable measurements (Schwartz, 2006). Given the dearth of 1906 geomorphic offsets, it is not surprising that studies along the 1906 rupture have not reported small channels or other surface features that show cumulative offsets for the past several earthquakes such as observed, for example, along the San Andreas fault in the Carrizo Plain (Sieh, 1978; Zielke *et al.*, 2010).

There are, however, some offset estimates from paleoseismic studies. Baldwin *et al.* (2000) exposed a buried paleochannel margin in trenches excavated parallel to the San Andreas fault at Alder Creek near Point Arena on the North Coast segment (Fig. 2). They interpret the channel to be offset by two ruptures, 1906 and the penultimate. They measured a net offset of the channel margin of 8.0–9.5 m. Baldwin *et al.* (2000) note that in 1906 a 4.9 m offset was reported 1.2 km south of this site. Accounting for uncertainties in projection of the channel margin to the fault and subtracting the nearby amount of 1906 offset, Baldwin *et al.* (2000) measure a penultimate northern San Andreas offset of 3.1–4.6 m.

At the Filoli site on the Peninsula segment of the fault (Fig. 2), Hall *et al.* (1999) reconstructed buried stream channels offset by the San Andreas. They conclude that a channel with a radiocarbon age of  $330 \pm 200$  yr B.P. is offset  $4.1 \pm 0.5$  m. This is interpreted as recording 2.5 m ( $\pm 0.2$ ) of surface slip that occurred at this location in 1906 and  $1.6 \pm 0.7$  m of slip in the penultimate rupture, which they contend is 1838.

#### Rodgers Creek Fault

The Rodgers Creek fault exhibits intermittent geomorphic expression of the most recent event in the form of short scarplets, small left stepping en echelon pushups, sharp linear furrows, and at least one offset channel. Much of this fault geomorphology is being modified by grazing, grape planting, and slope processes. The clearest evidence of the amount of slip during the most recent event is at the Beebe Ranch (Fig. 2). A channel with an associated debris flow levy on its south margin was right-laterally offset 2 m ( $0.2, +0.3$ ) during the most recent rupture (Budding *et al.*, 1991). In 2000, a debris flow filled this channel and modified its geometry.

At the Triangle G site (Fig. 2), 0.7 km to the north, the fault is expressed as a short pressure ridge. Hecker *et al.* (2005) reconstruct the gradient of a buried debris flow offset along the northeast trace of the fault during the most recent

surface rupture. Their estimate of 2.2 m (+1.2, 0.8) of right-lateral slip along the northeast side of the pressure ridge is a minimum for the site because an unknown amount of additional slip occurred on the fault flanking the southwest side of the ridge. They conclude the amount of slip at the Triangle G Ranch site during this event is similar to, but probably larger than, the surface offset measured for the same rupture at Beebe Ranch.

There is also evidence that multimeter single event offsets occurred during ruptures prior to the most recent event. At Beebe Ranch, Budding *et al.* (1991) correlate buried channels across the fault exposed in fault-parallel trenches. This provides an estimate of net offset of 5.1–7.2 m. Radio-carbon dating at the Beebe Ranch and at Triangle G indicates that this offset represents three ruptures (Schwartz *et al.*, 1992). Removing slip from the most recent event leaves anywhere from 2.8 to 5.4 m for the penultimate and prepenultimate ruptures at this location.

### San Gregorio Fault

Simpson *et al.* (1997) combine trench and site mapping relations to estimate slip during both the most recent and the penultimate surface rupture across the San Gregorio fault at Seal Cove (Fig. 2). Each event occurred on a different fault strand and the offsets were measured separately. The most recent San Gregorio surface rupture extends through a Native American midden that was mapped using 145 hand auger borings. Simpson *et al.* (1997) conclude that it is deflected across the fault 5 m (2, +6). For the penultimate event, Simpson *et al.* (1997) reconstructed the geometry of a wedge of offset terrace sand, and they estimate slip of  $3.0 \pm 0.2$  m.

### Hayward Fault

There are no geologically measured horizontal slips per event data for the Hayward fault. Surface rupture did occur during 1868, as reported in Lawson (1908), extending at least 36 km from San Leandro to Warm Springs. Although the location of “the crack” (as the fault trace is primarily referred to in Lawson, 1908) is described, references to offset are vague. In some places it exhibited displacement of 8 or

10 inches and in others “a displacement of 3 feet is said to be observed” (Lawson, 1908, p. 435). Yu and Segall (1996) geodetically modeled the 1868 rupture, suggesting a length of 45–60 km and an average displacement of 1.9 m ( $\pm 0.4$ ).

In their investigation of the southern Hayward fault at Tyson’s Lagoon (Fig. 2), Lienkaemper *et al.* (2002) measure vertical separation for the past four ruptures. Based on the thickness of small colluvial wedges adjacent to the main fault trace, they estimate a vertical component of slip of 0.1–0.2 m for 1868 and 0.3, 0.2, and 0.45 m for the penultimate, third, and fourth events back, respectively. Lienkaemper *et al.* (2002) conclude that if the horizontal-to-vertical ratio of slip remains generally constant, then the similarity of vertical displacement for the past four Tyson Lagoon events suggests generally similar horizontal slip at this location.

U.S. Geological Survey  
345 Middlefield Road  
Menlo Park, California 94025  
(D.P.S., J.J.L., S.H., T.E.F.)

URS Corporation  
1333 Broadway  
Oakland, California 94612  
(K.I.K.)

Lettis Consultants International  
1981 N. Broadway  
Walnut Creek, California 94596  
(J.N.B.)

California Geological Survey  
345 Middlefield Road  
Menlo Park, California 94025  
(G.G.S.)

Department of Geosciences  
University of Missouri-Kansas City  
5100 Rockhill Road  
Kansas City, Missouri 64110  
(T.M.N.)

Manuscript received 29 October 2012;  
Published Online 20 May 2014